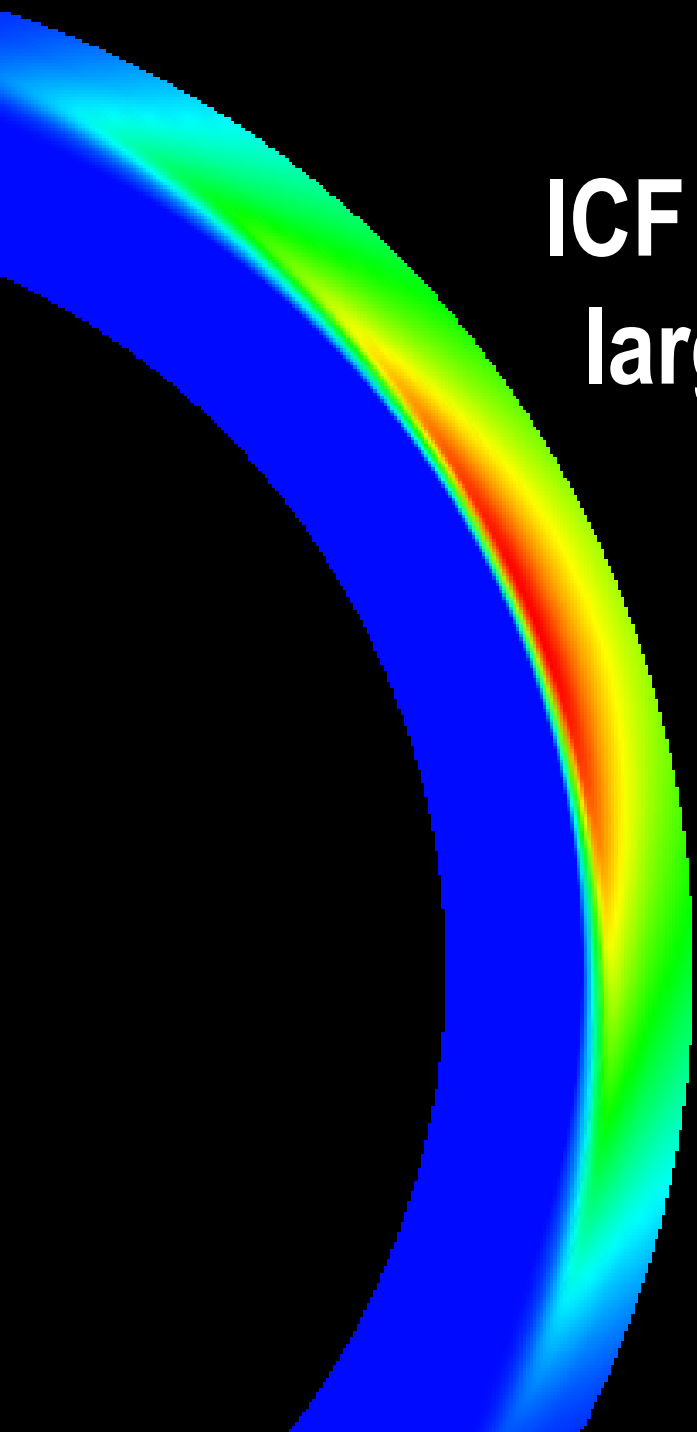

ICF modelling of interaction of large heavy ion beams with a target

A. Ogoyski, S. Kawata and A. Blagoev

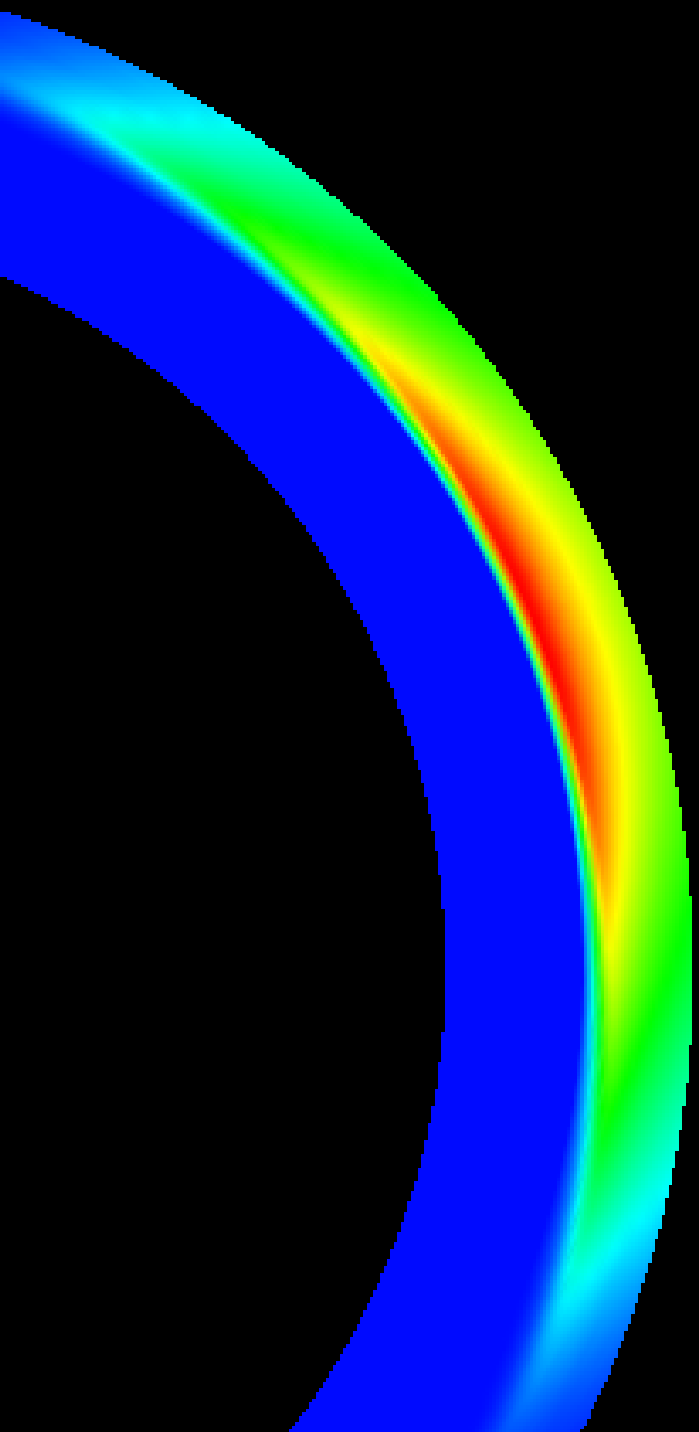

Main purposes:

1. To clarify multi-beam energy deposition process in HIF.
2. To simulate a little pellet displacement from the chamber center and to analyze its result on the energy deposition uniformity.
3. To optimize HIB irradiation system and fuel pellet structure.

Physics model: *Stopping Power*

$$\mathrm{E_{StPower}} = \mathrm{E_{nuc}} + \mathrm{E_{bound}} + \mathrm{E_{free}} + \mathrm{E_{ion}}$$

1) $$\mathrm{E_{nuc}} = 10^{-7} C_{n1} \sqrt{E} \exp\left(-45.2\left(C_{n2}E\right)^{0.277}\right)$$

$$C_{n1} = 4.14\times10^{6}\rho\left(\frac{\mathrm{A_b}}{\mathrm{A_b}+\mathrm{A_t}}\right)^{3/2}\left(\frac{\mathrm{Z_b Z_t}}{\mathrm{A_t}}\right)^{1/2}\left(\mathrm{Z_b}^{2/3}+\mathrm{Z_t}^{2/3}\right)^{-3/2}$$

$$C_{n2} = 10^{-6}\left(\frac{\mathrm{A_b A_t}}{\mathrm{A_b}+\mathrm{A_t}}\right)^{3/2}\left(\mathrm{Z_b Z_t}\right)^{-1}\left(\mathrm{Z_b}^{2/3}+\mathrm{Z_t}^{2/3}\right)^{-1/2}$$

- ✓ effective in the end of the stopping range
- ✓ ion – target nucleus Coulomb collisions

2) $$\mathrm{E_{bound}} = \mathrm{E_{LSS}} \cup \mathrm{E_{Bethe}} \qquad \mathrm{Z_b}^{1/3} \geq 137\frac{\mathrm{V_{beam}}}{c}$$

$$\mathrm{E_{LSS}} = \frac{2e^2 a_B n_{eb}}{\varepsilon_0 V_B}\frac{\mathrm{Z_b}^{7/6}}{\left(\mathrm{Z_b}^{2/3}+\mathrm{Z_t}^{2/3}\right)^{3/2}}\mathrm{V_{beam}} \qquad \beta = \frac{\mathrm{V_{beam}^2}}{c^2}$$

$$\mathrm{E_{Bethe}} = \frac{e^4 n_{eb}}{4\pi\varepsilon_0^2 m_e}\frac{Zeff_b^{\,2}}{\mathrm{V_{beam}^2}}\left[\ln\frac{2m_e\mathrm{V_{beam}^2}}{\langle U_i\rangle} - \ln(1-\beta) - \beta - \delta\right]$$

$$Zeff_b = \mathrm{Z_b}\left(1 - 1.034\exp\left(-137.04\frac{1}{\mathrm{Z_b}^{0.69}}\frac{\mathrm{V_{beam}}}{c}\right)\right)$$

- ✓ Thomas – Fermi description of the electron clouds
- ✓ excitation and ionization processes
- ✓ ion – bound electron Coulomb collisions
- ✓ Brown and Moak expression for $Zeff_b$

3) $$\mathrm{E_{free}} = \frac{e^4 n_{ef}}{4\pi\varepsilon_0^2 m_e}\frac{Zeff_b^{\,2}}{\mathrm{Vr_e^2}}\left(G_e L_e + H_e\right)$$

$$G_e = \mathrm{erf}\left(\frac{\mathrm{X_e}}{\sqrt{2}}\right) - \sqrt{\frac{2}{\pi}}\mathrm{X_e}\exp\left(-\frac{\mathrm{X_e^2}}{2}\right) \qquad L_e = \ln\left(\frac{\lambda_D}{b_{min}}\right)$$

$$H_e = -\frac{\mathrm{X_e^3}}{3\sqrt{2\pi}}\exp\left(-\frac{\mathrm{X_e^2}}{2}\right) + \frac{\mathrm{X_e^4}\ln\mathrm{X_e}}{\mathrm{X_e^4}+12} \qquad \mathrm{X_e} = \frac{\mathrm{Vr_e}}{\mathrm{V_e}}$$

- ✓ becomes effective with target temperature growth
- ✓ G_e is the Chandrasechar function

4) $$\mathrm{E_{ion}} = \frac{e^4 n_a}{4\pi\varepsilon_0^2 M_t}\frac{Zeff_b^{\,2} Z_t^2}{\mathrm{V_{beam}^2}}\left(G_i L_i + H_i\right)$$

$$G_i = \mathrm{erf}\left(\frac{\mathrm{X_i}}{\sqrt{2}}\right) - \sqrt{\frac{2}{\pi}}\mathrm{X_i}\exp\left(-\frac{\mathrm{X_i^2}}{2}\right) \qquad L_i = \ln\left(\frac{\lambda_D}{b_{min}}\right)$$

$$H_i = -\frac{\mathrm{X_i^3}}{3\sqrt{2\pi}}\exp\left(-\frac{\mathrm{X_i^2}}{2}\right) + \frac{\mathrm{X_i^4}\ln\mathrm{X_i}}{\mathrm{X_i^4}+12} \qquad \mathrm{X_i} = \frac{\mathrm{V_{beam}}}{\mathrm{V_i}}$$

- ✓ becomes effective in high target compression and temperature

Physics model: *Target Temperature*

$$N_b E_b = E_{dst} + E_i + E_{rad} + n_{Al} V_{dp} \frac{3}{2}(T_m - T_0)$$

$$E_{dst} = n_{Al} V_{dp} E_{cpl}$$

$$E_i = n_{Al} V_{dp} \langle I \rangle \frac{1}{T_m - T_0} \int_{T_0}^{T_m} Z(T) dT$$

$$E_{rad} = \sigma S \int_0^{t_{dp}} T^4(t) dt$$

$$Z(T) = \frac{13.2\ T}{259.6 + T}$$

- ✓ E_{dst} – energy loss for destruction of the initial crystal state of the target.
- ✓ E_i – ionization loss in the target.
- ✓ E_{rad} – radiation loss across the target surface *S*.
- ✓ $\langle I \rangle$ – ionization potential of the target.
- ✓ σ – Stephan-Boltzmann constant.
- ✓ t_{dp} – deposition time
- ✓ $Z(T)$ – target ionization, that was evaluated by solving the EOS using TF model and interpolating results for a fixed solid state density.

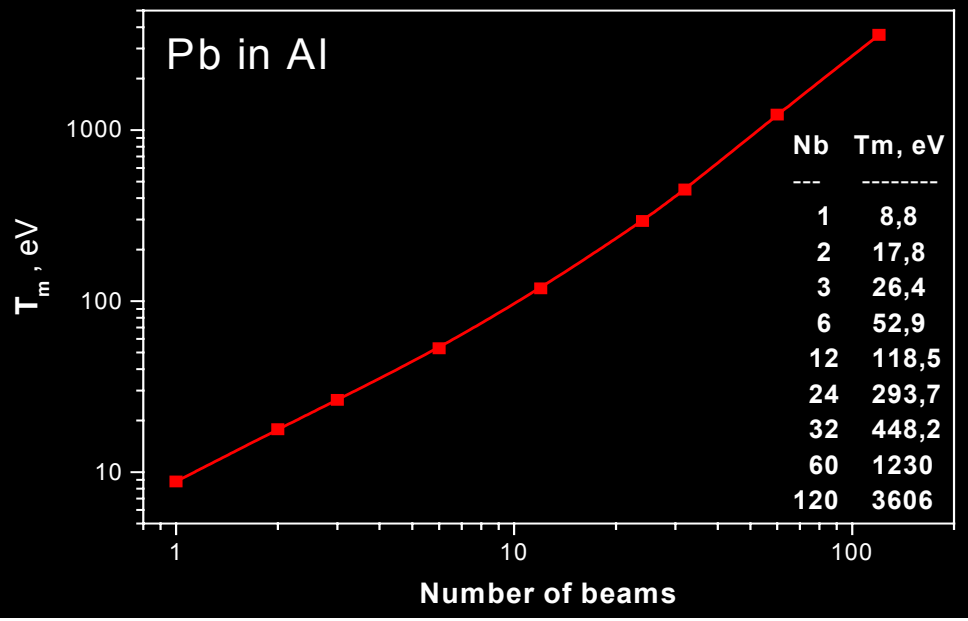

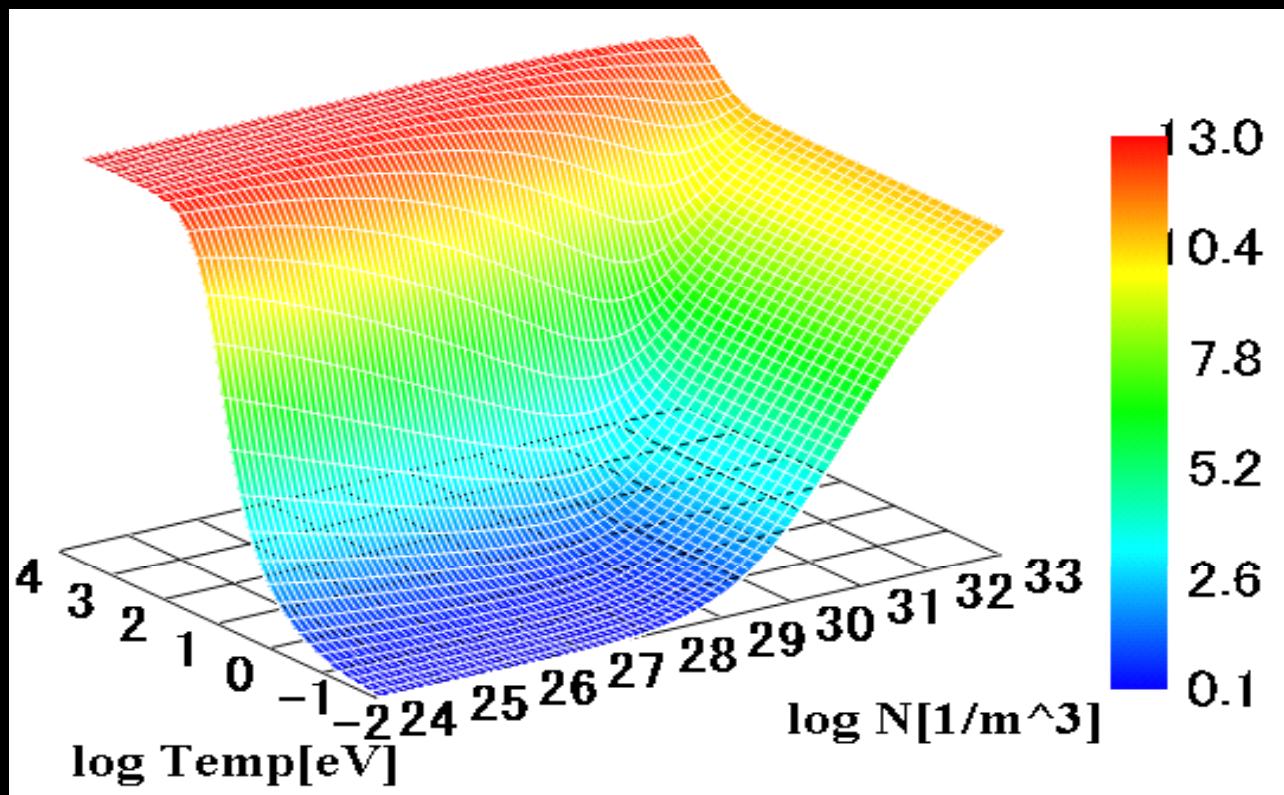

Physics model

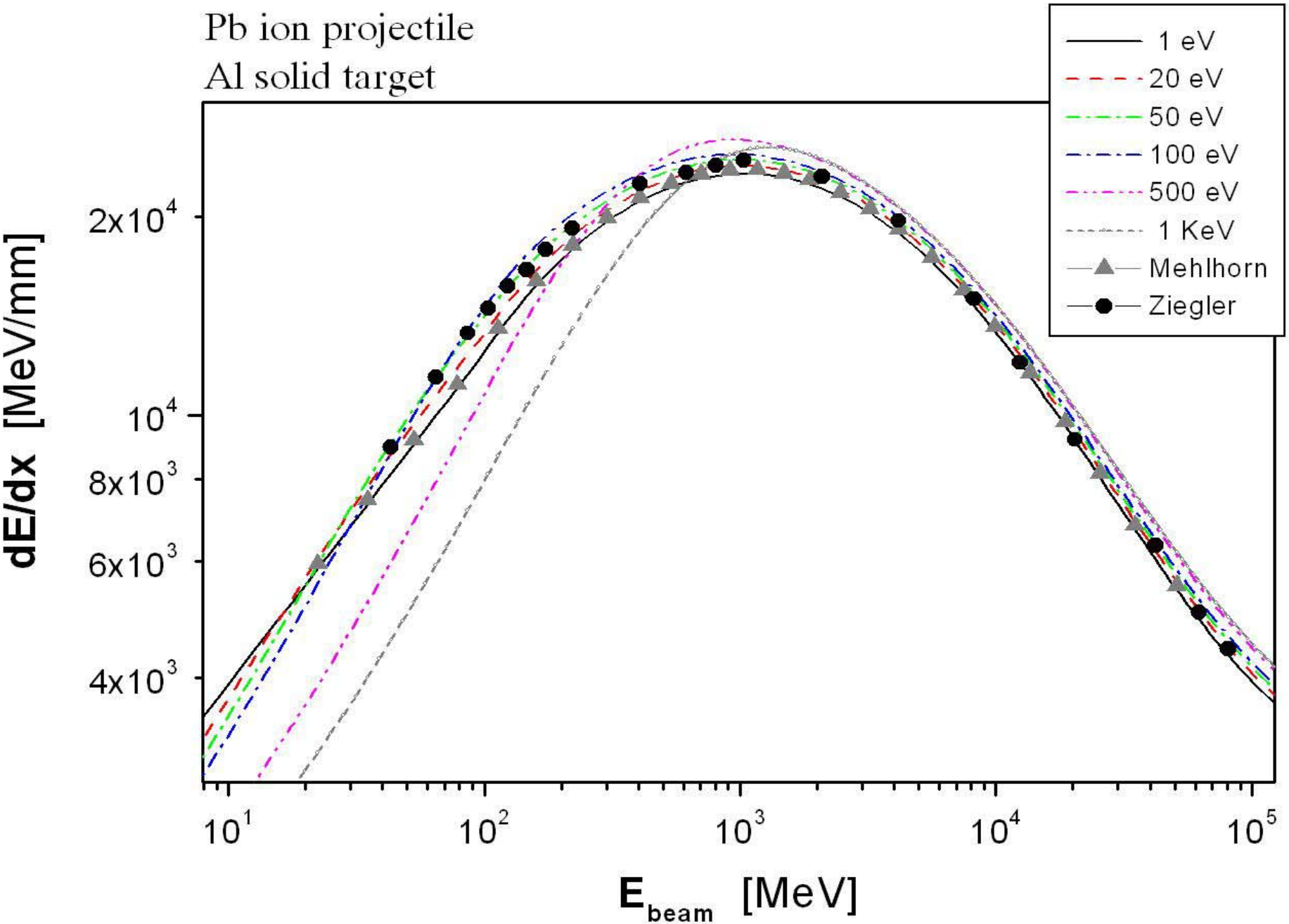

Simulation model

- Pb^{+} ion beams in Al target R 4 mm
- prt. number distribution : K-V, Gauss
- prt. energy distribution : Maxwell
- max. prt. density: $1{,}3\times10^{11}\,cm^{-3}$
- prt. mean energy: 8 GeV (38,6 MeV/u)
- maximal current: 5 kA
- pulse width: 10 ns
- beam radius R_{en} : 35 mm – 3,6 mm
- chamber radius: 2 – 8 m
- beam emittance: 3 – 10 mm-mrad
- linear T_{trg} growth: 0,025 – 8,8 eV for 1 b
  0,025 – 448 eV for 32 b

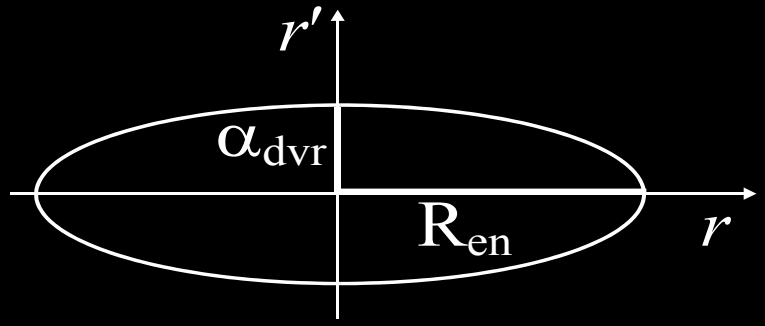

(a)

$$\varepsilon_r = \iint dr\, dr' = \pi \alpha_{dvr} R_{en} = \frac{\pi^2}{0.18} R_{en} \tan^{-1}\left(\frac{R_f}{R_{ch}+f}\right)$$

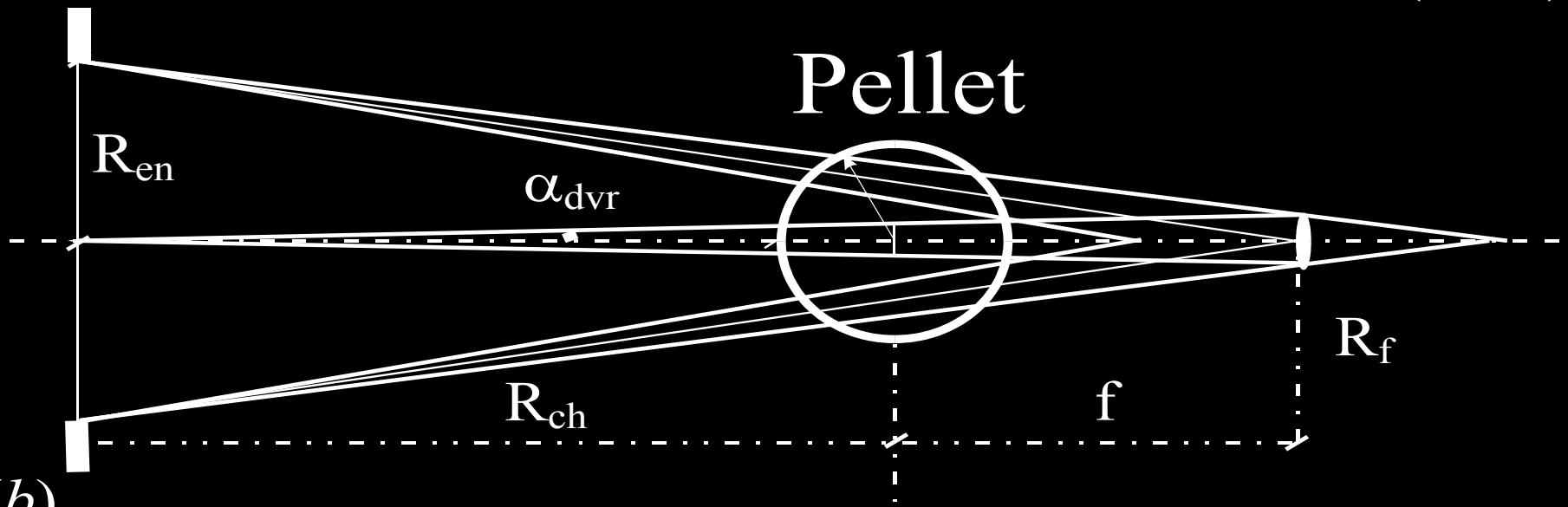

(b)

One Pb beam energy deposition in Al monolayer structure

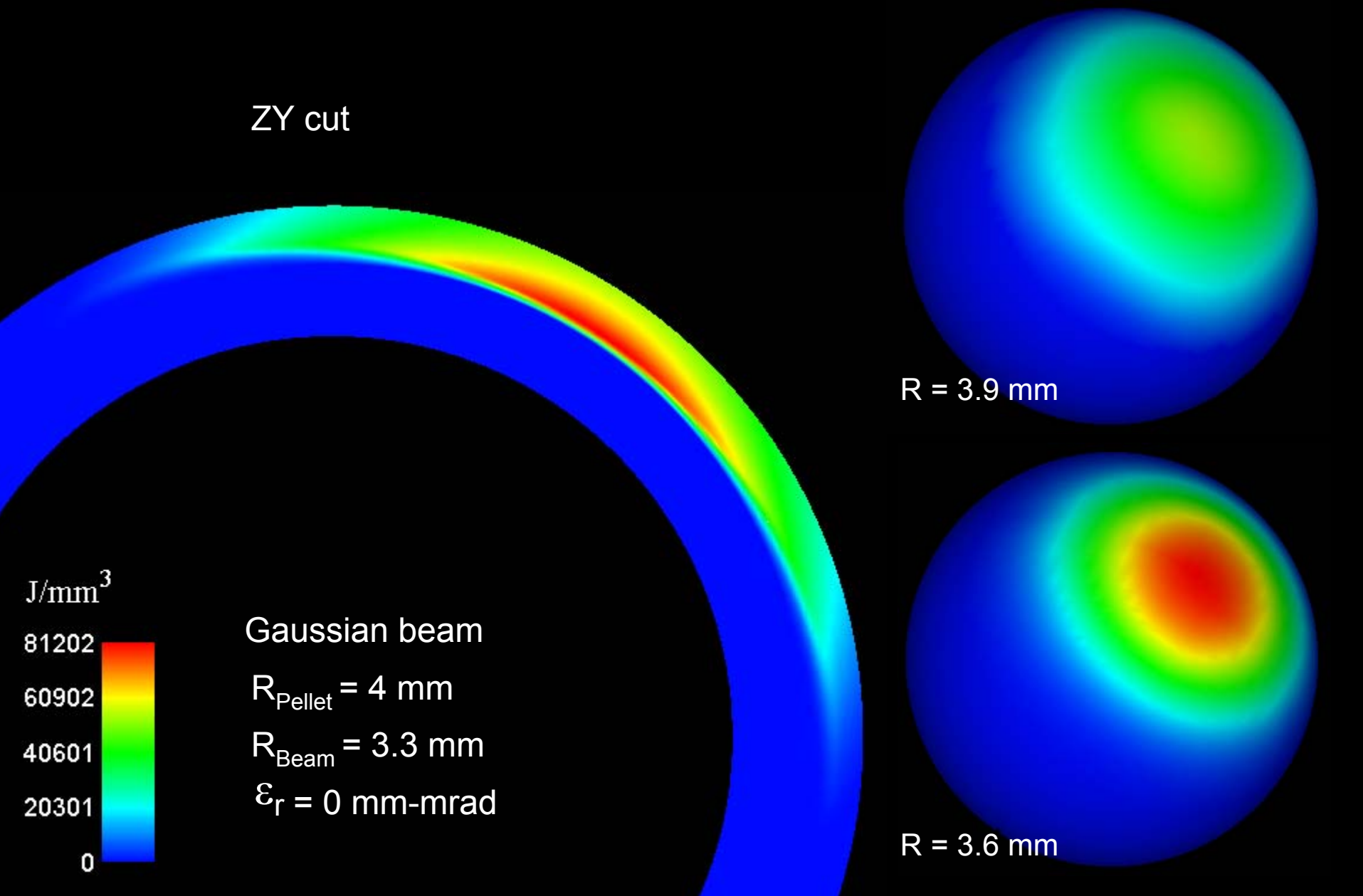

One Pb beam energy deposition in Al monolayer structure

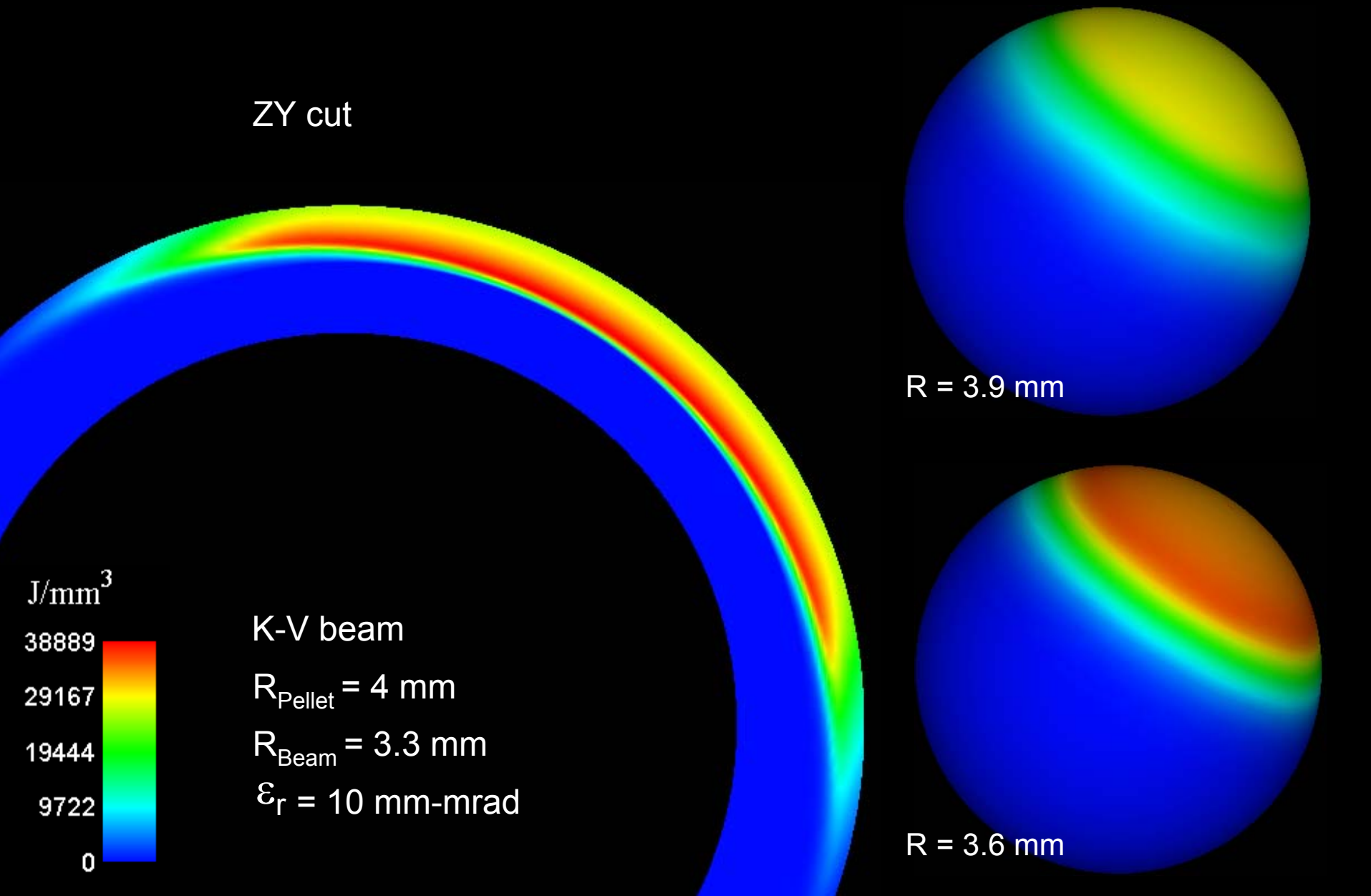

One Pb beam energy deposition in Al monolayer structure

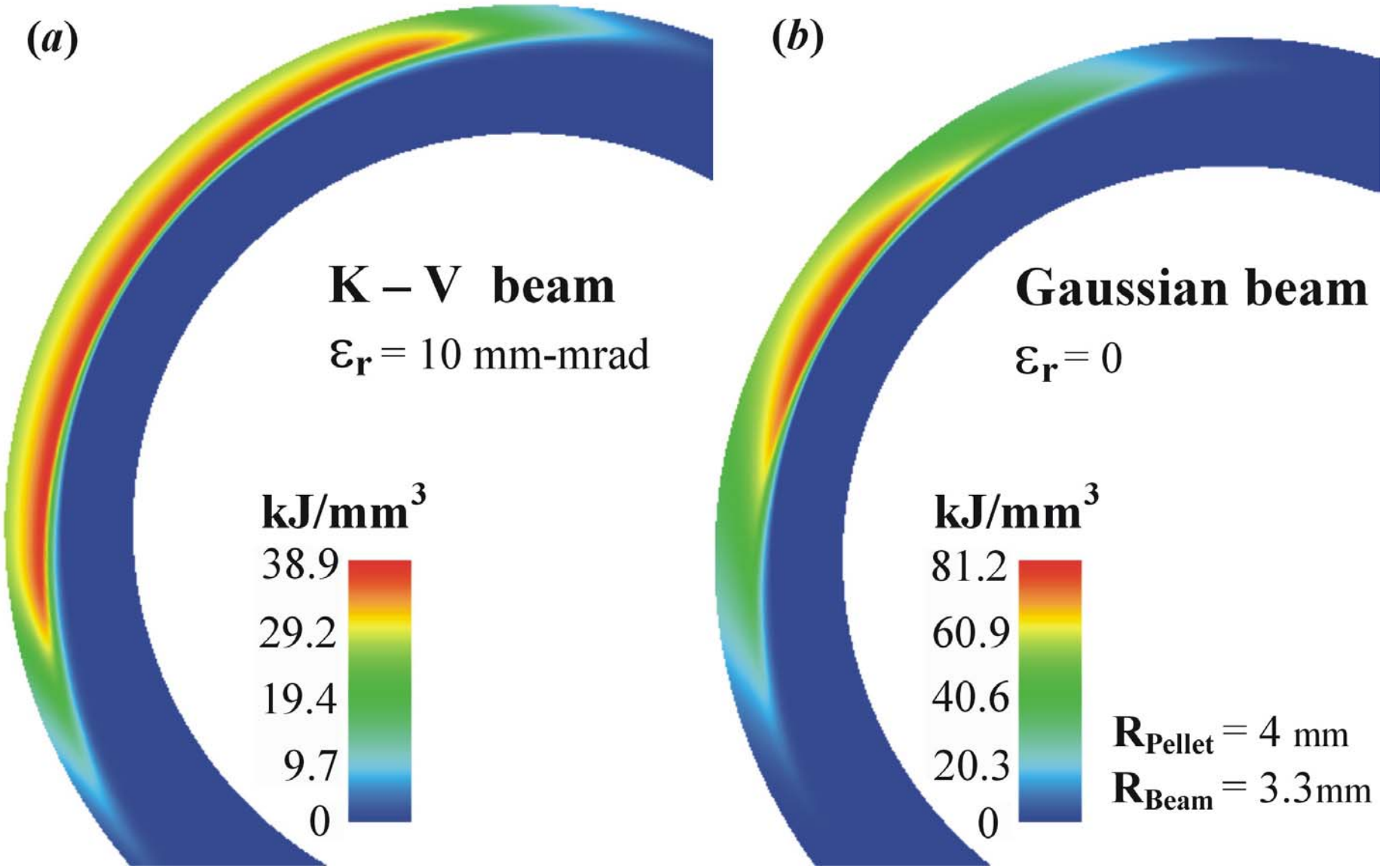

Non-uniformity estimation

- Total r-m-s deviation: $\sigma_{\text{rms}} = \sum_i^{n_r} w_i \sigma_i \quad , \quad \sigma_i = \frac{1}{\langle E \rangle_i} \sqrt{\frac{\sum_j^{n_\theta} \sum_k^{n_\phi} \left(\langle E \rangle_i - E_{ijk} \right)^2}{n_\theta n_\phi}}$

- Total p-t-v deviation: $\sigma_{\text{ptv}} = \sum_i^{n_r} w_i \sigma_i^I \quad , \quad \sigma_i^I = \frac{E_i^{\max} - E_i^{\min}}{2\langle E \rangle_i} \quad , \quad w_i = \frac{E_i}{E}$

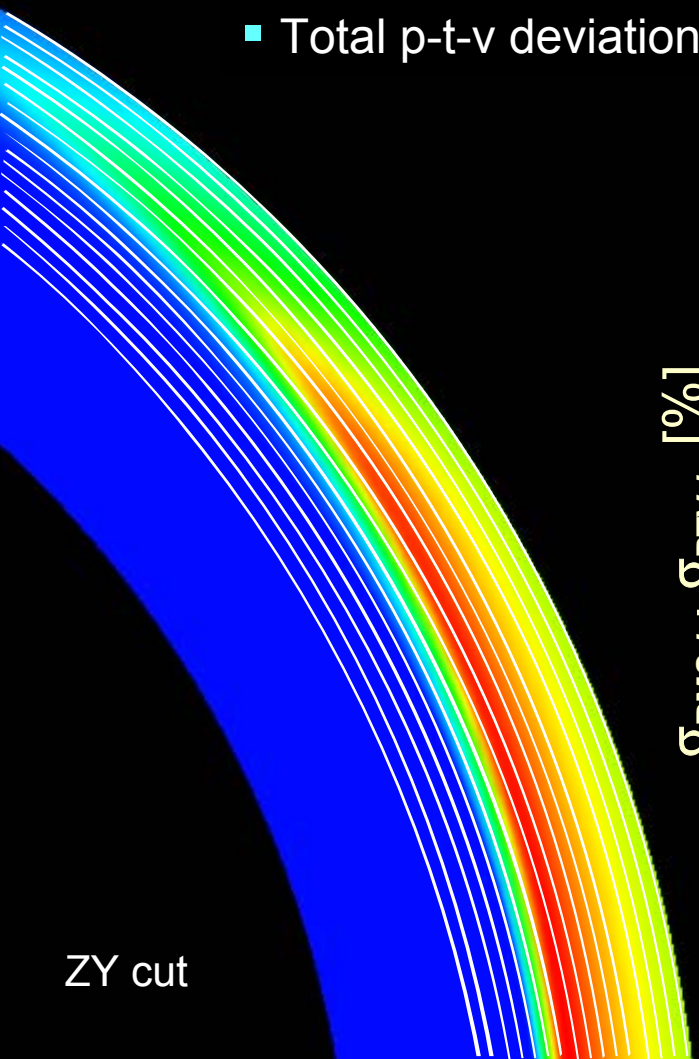

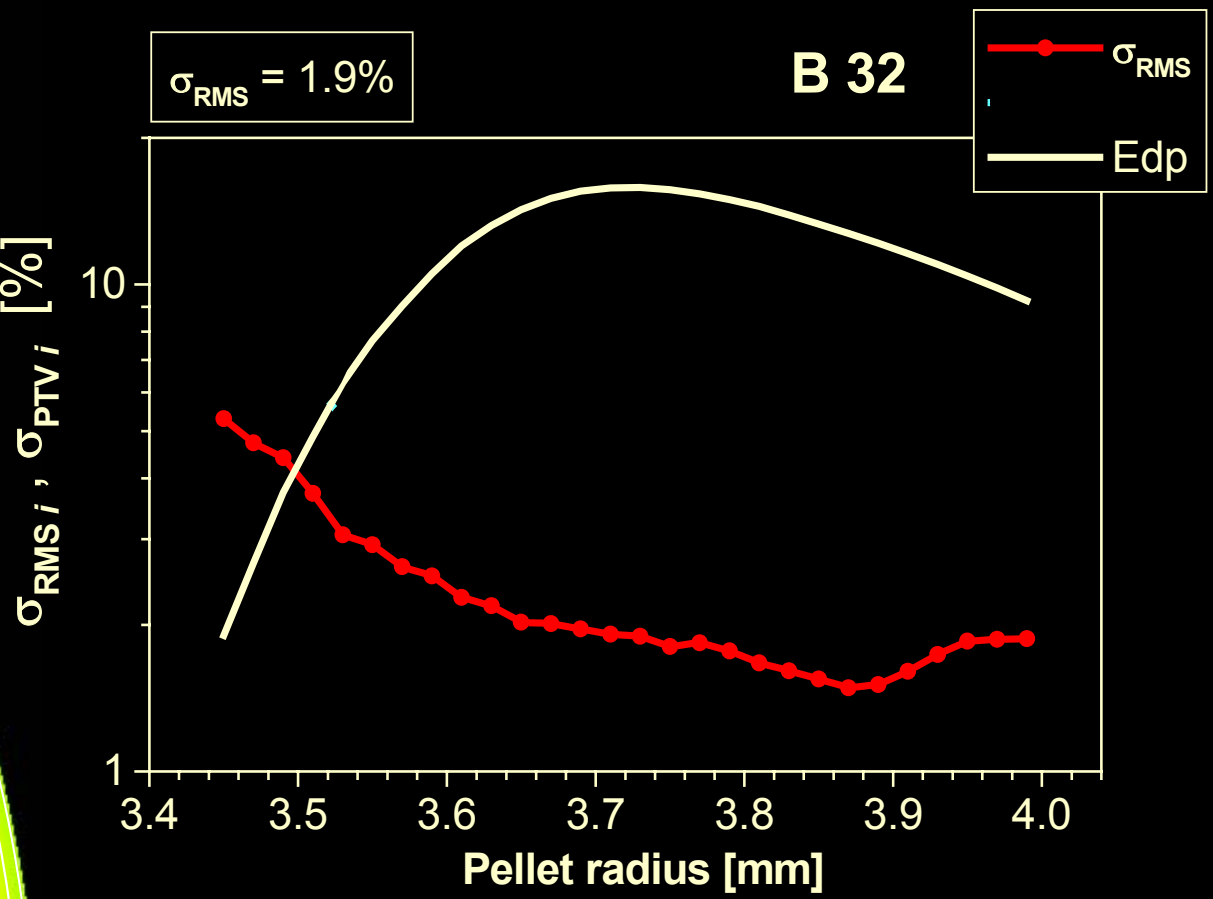

Beam number influence on the energy deposition non-uniformity

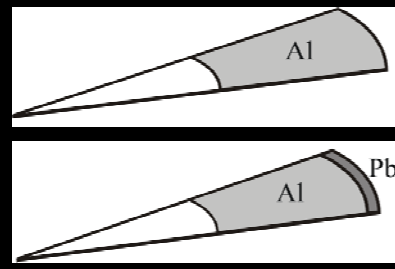

R_{ch} = 2 m ε_r = 10 mm-mrad

Pb – Al pellet

Al

Pb-Al

σ_{RMS} [%]

10

1

10

100

Beam Number

Pellet displacement sensitivity in total energy deposition

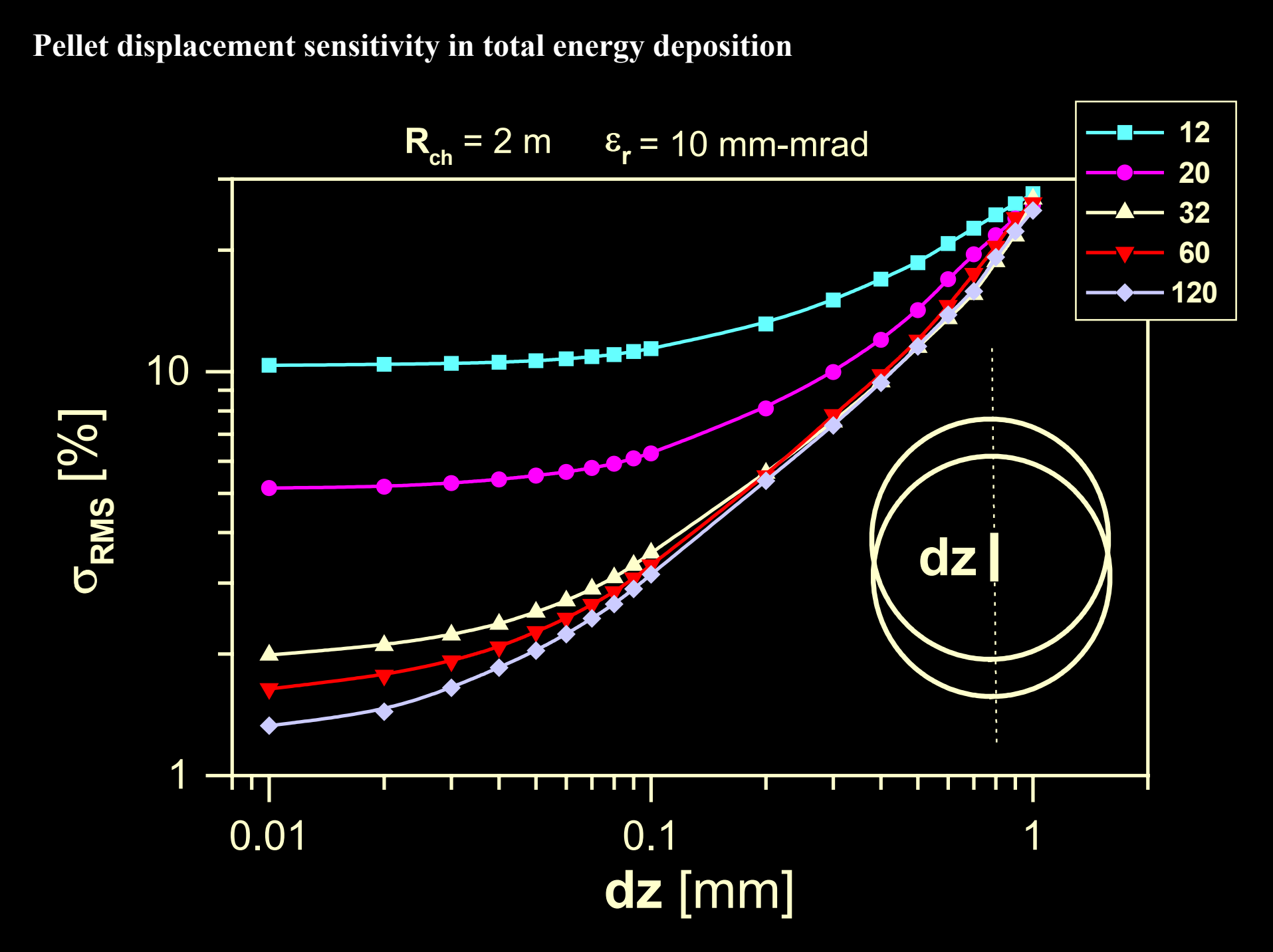

Pellet displacement sensitivity in total energy deposition

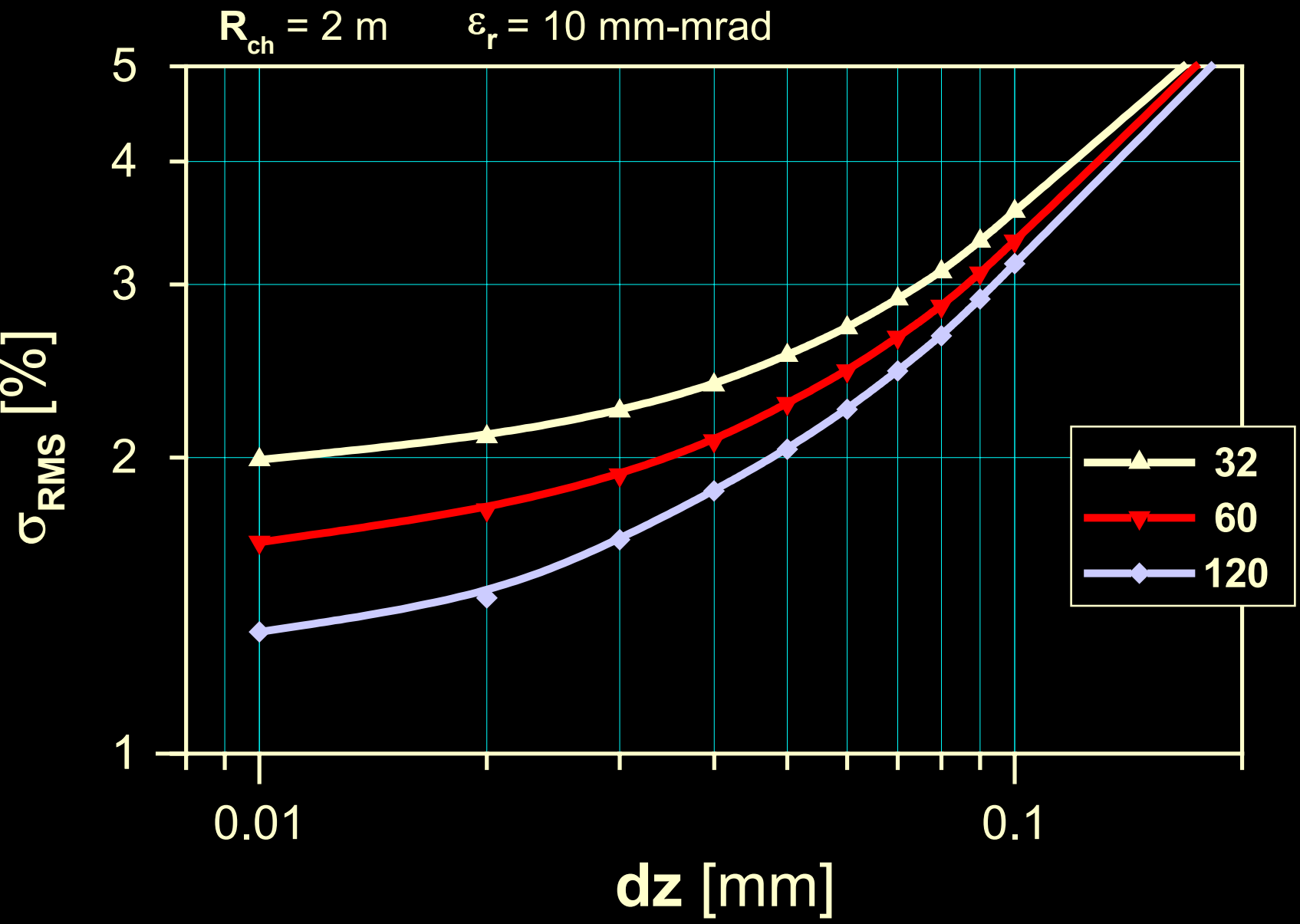

Pellet displacement sensitivity decreasing by using of large HIBs

The idea consists in two essential points:

1) Using of large ion beams
(beam radius > pellet radius).

2) Modifying irradiation scheme from spherical symmetric to axial symmetric in order to obtain an ellipsoidal area in the reactor chamber where the energy deposition non-uniformity to remain nearly constant if the pellet is inside.

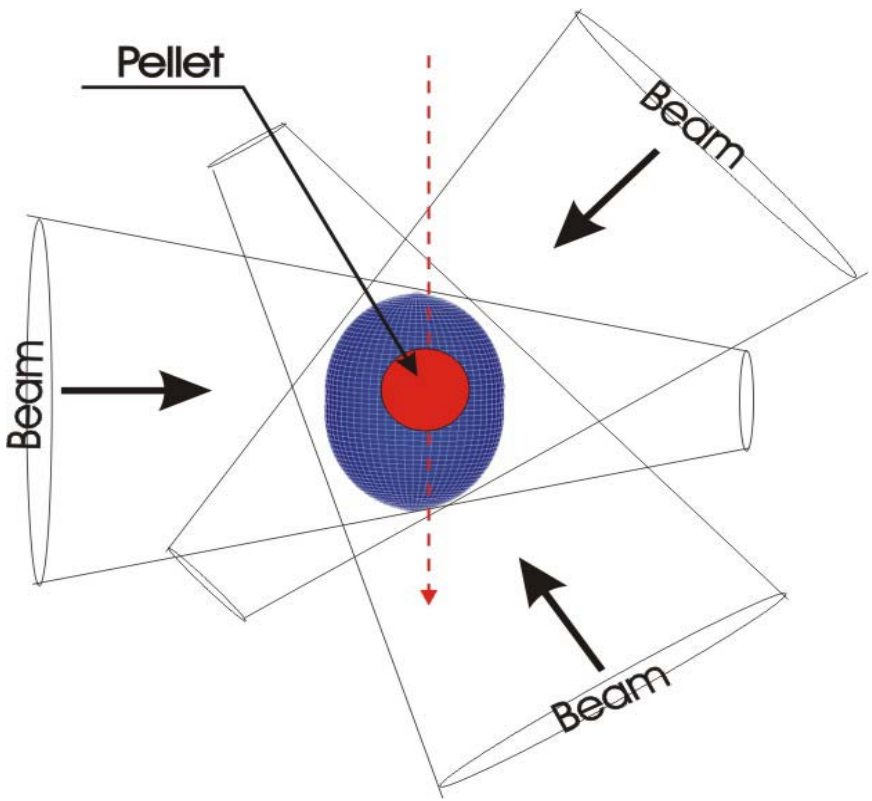

OMEGA-32 spherical symmetric scheme

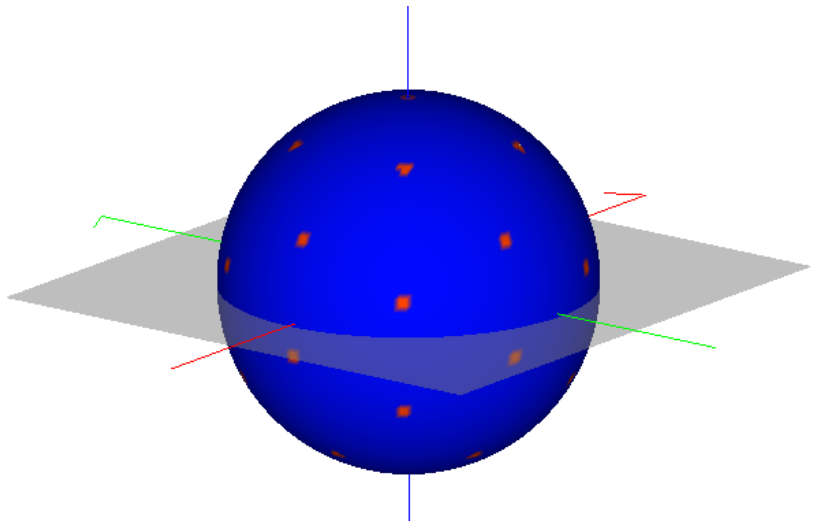

OS-32 modified axial symmetric scheme

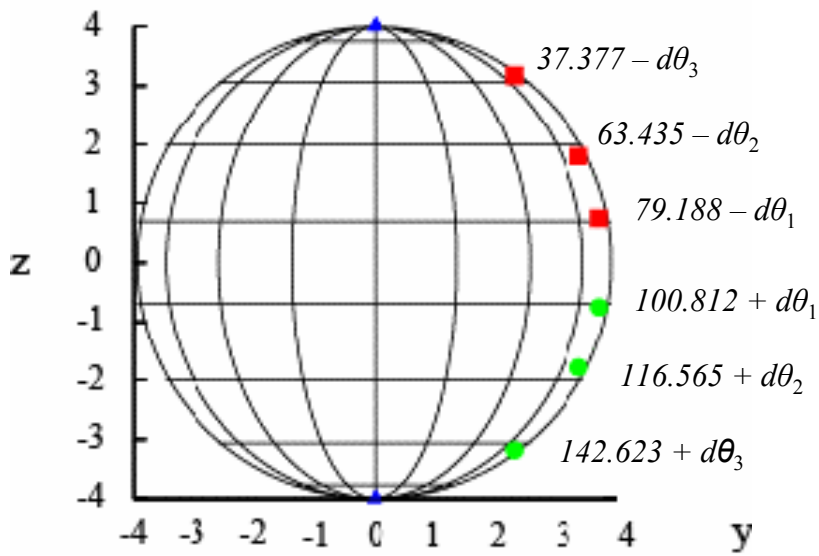

Pellet displacement sensitivity results

1) HIB parameters:
-32 Pb^{+} ion beams
-maximum current: 5kA
-mean particle energy: 8 GeV
-pulse width: 10 ns,
-beam length: 837 mm,
-maximal initial beam density: 1.3 x 10^{11} cm^{-3}
-beam radius at the chamber entrance: 35mm
-beam radius near to the pellet surface: 5.6mm
-chamber radius: 5m
-beam particle density distribution: Gaussian
-beam temperature: 100 MeV in Maxwell dis.
-beam emittance: 10 mm-mrad

2) Pellet parameters:
-external pellet radius: 4mm
-material: Aluminum
-shape: spherical
-pellet temperature: linear growth during the time of deposition from 0.025 eV to 448 eV

3) OS-32 scheme parameters:
$d\theta_1=d\theta_2=d\theta_3$= 4deg

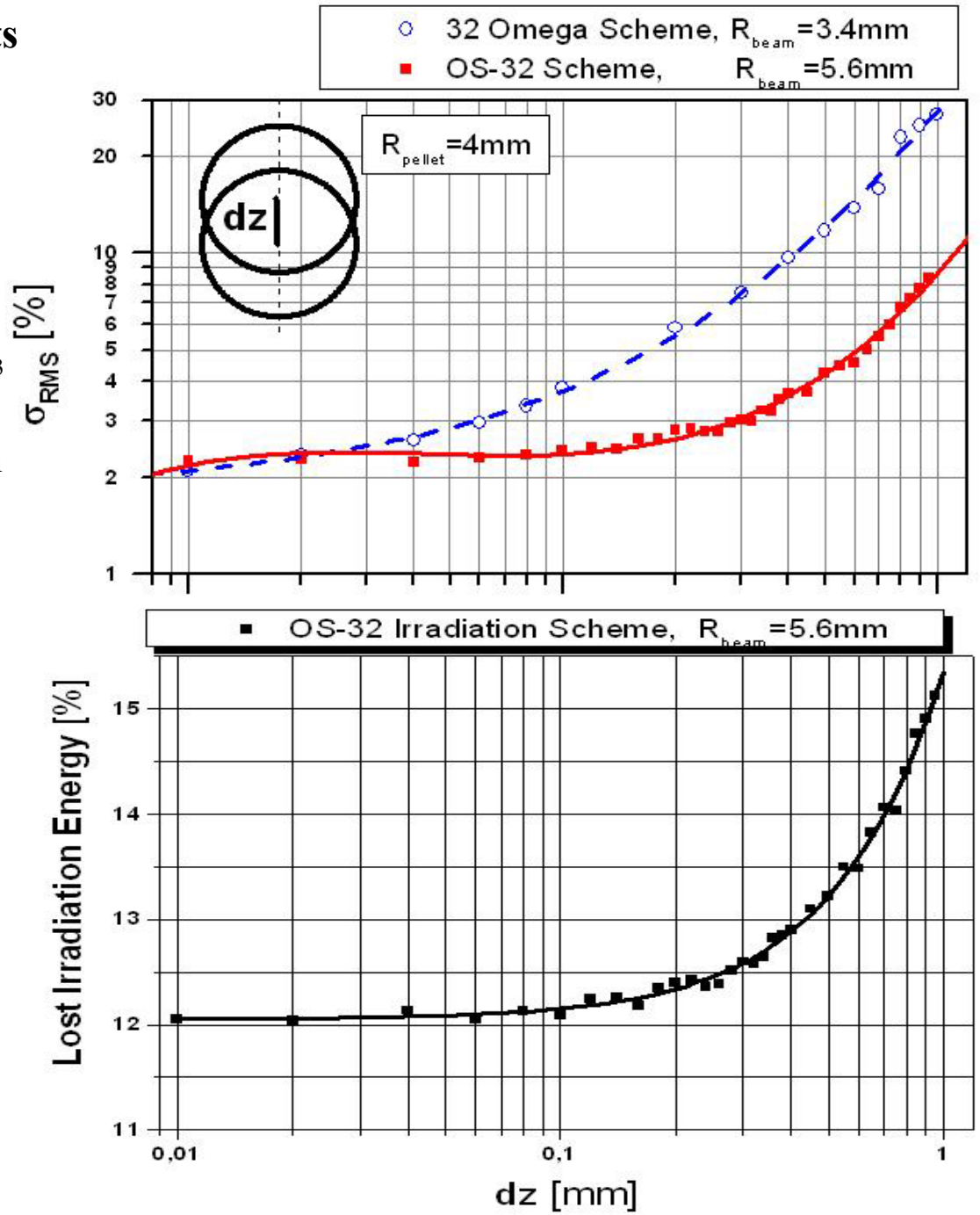

Kawata Lab results

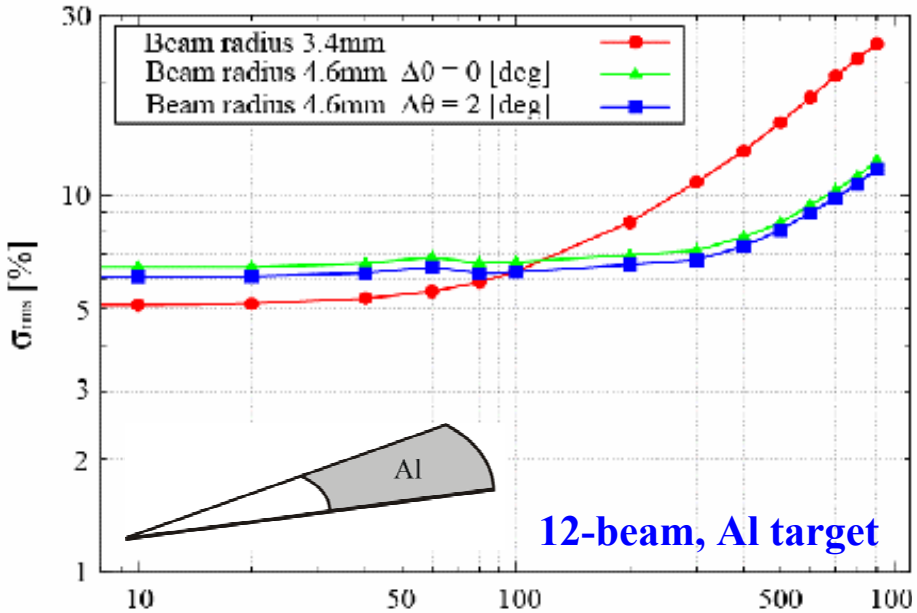

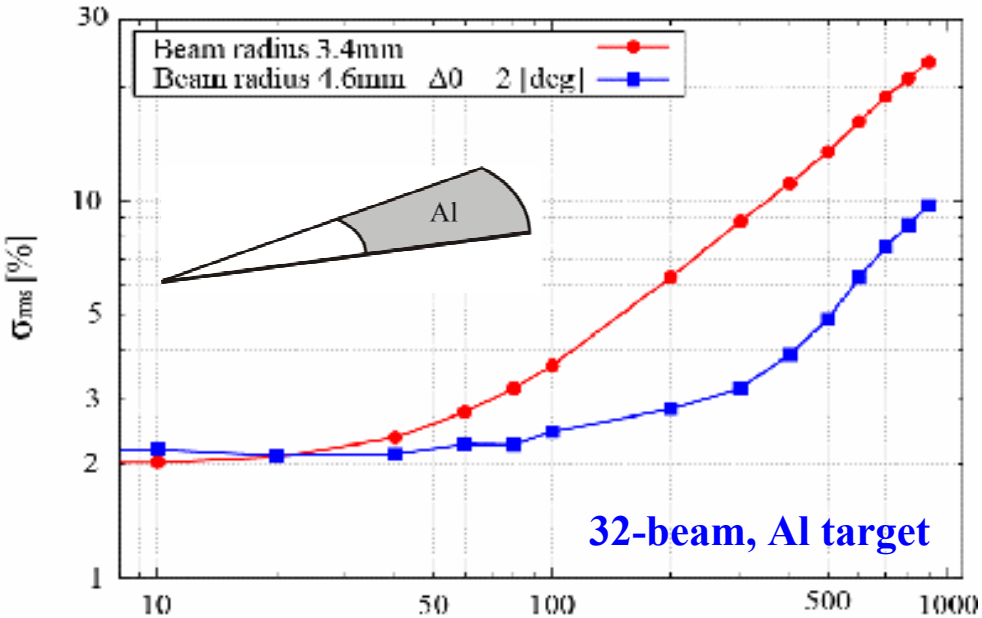

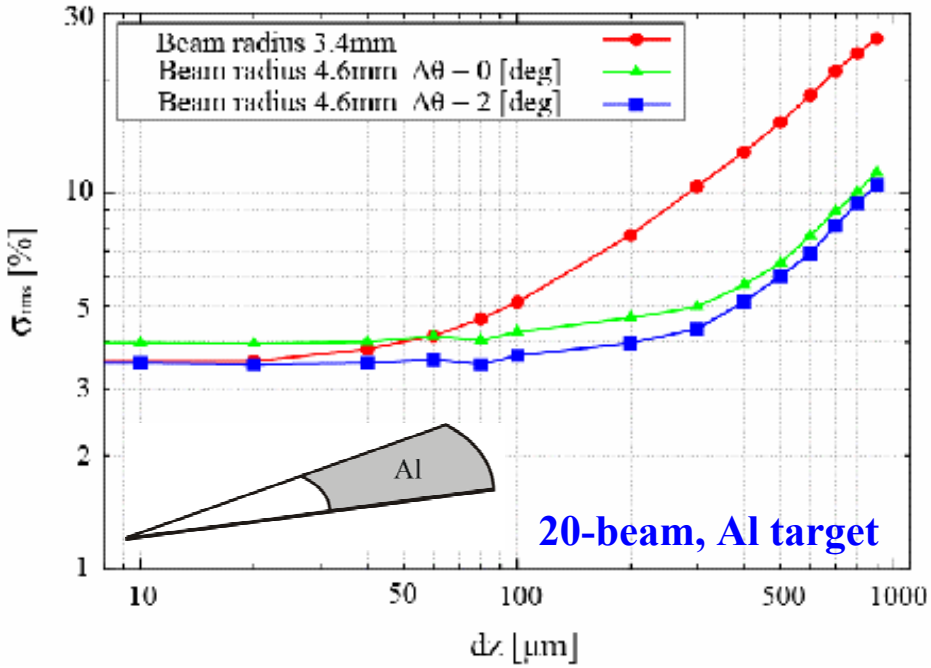

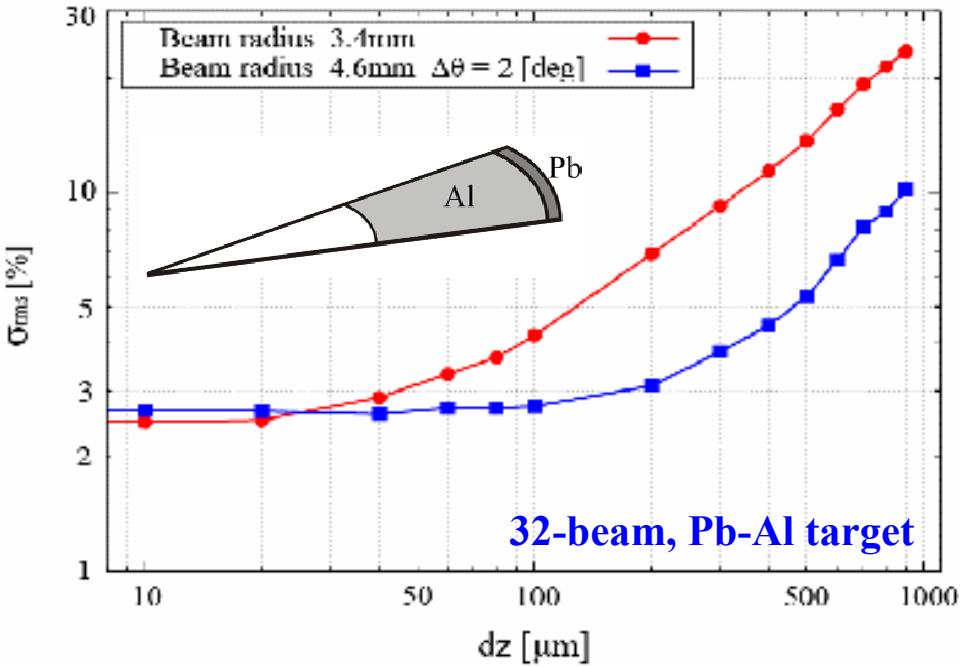

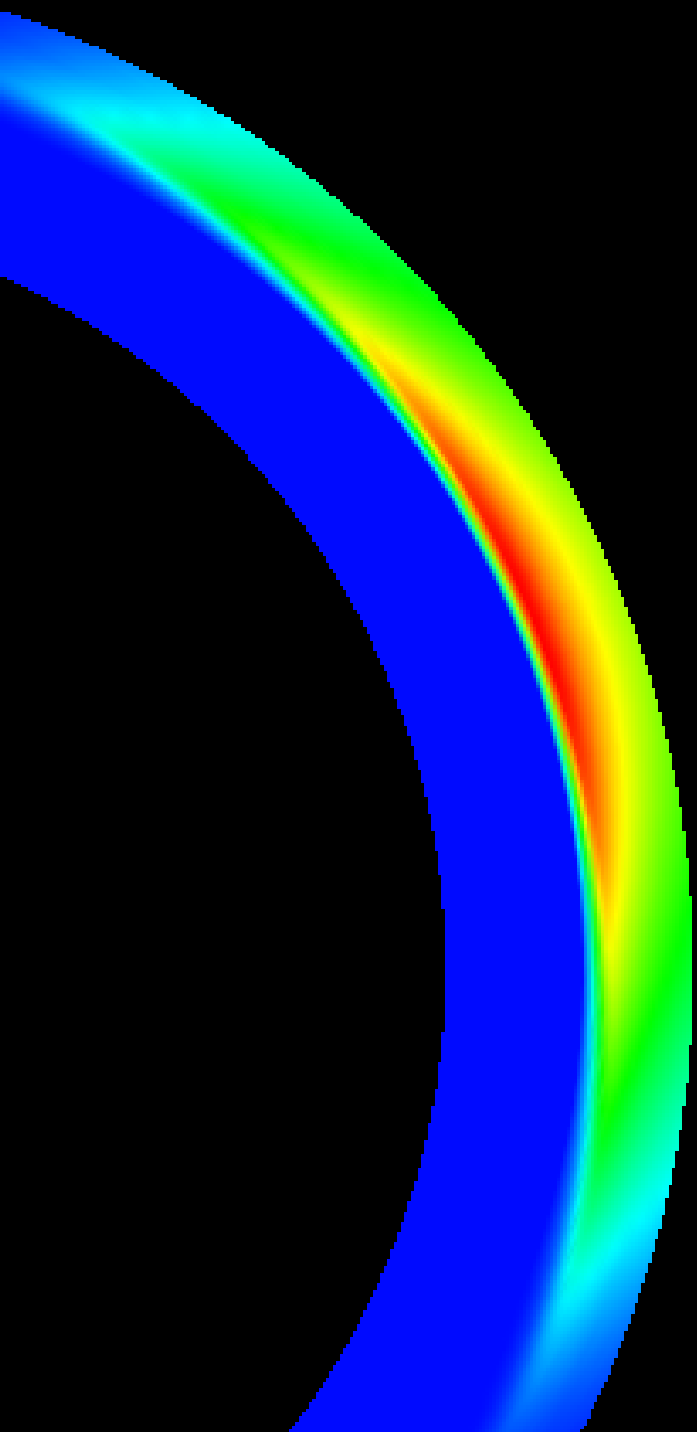

Summary:

1. Three-dimensional computer codes OK1, OK1c and OK2 were developed for simulation of multi HIB irradiation on a spherical, cylindrical and arbitrary shaped fuel pellet.
2. A 3D criterion for non-uniformity estimation was established.
3. We investigated the energy deposition non-uniformity dependence on:
   - reactor chamber radius,
   - beam focusing,
   - beam emittance,
   - beam number irradiation system,
   - little pellet displacement from the reactor chamber center.
4. A 32-beam irradiation scheme has been confirmed the most interesting for the future HIF practice.
5. A new OS-32 HIB irradiation scheme is proposed, robust against pellet displacement.

In case of additional discussions

additional

My questions

SIS 100: Uranium beam intensity of 2×10^{12} / bunch of 50 ns

E_{beam} 200 MeV/u; V_{beam} $1{,}7\times10^{8}$ m/s;

Particle number density $9{,}5\times10^{8}$ cm^{-3}

1) *Has the cross section of U ion collisions been evaluated?*

2) *Can we expect induced Uranium fission reactions in the end of the stopping range?*

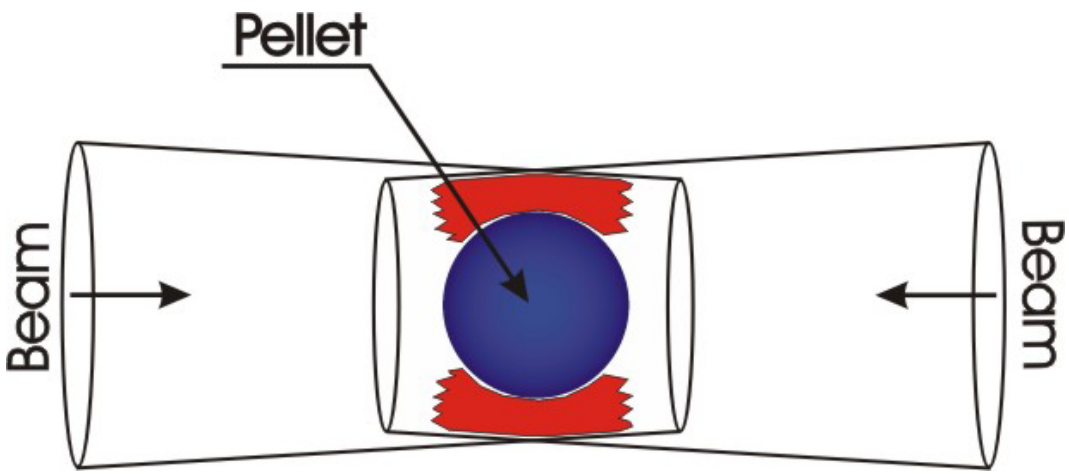

additional

Physics model

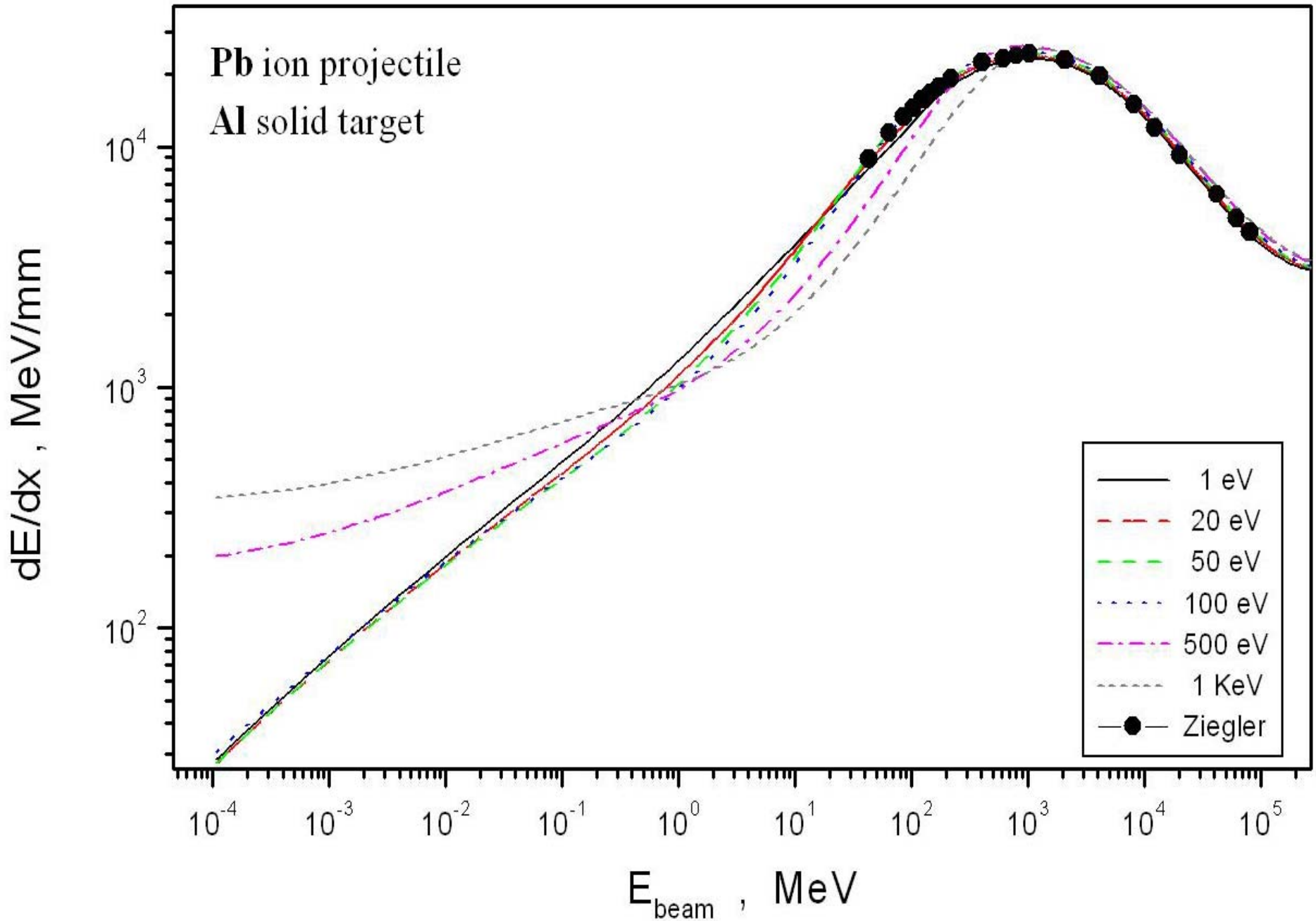

additional

Simulation model

- Pb^{+} ion beams in Al and Pb-Al target
- prt. number distribution : K-V, Gauss
- prt. energy distribution : Maxwell
- max. prt. density: $1.3\times10^{11}cm^{-3}$
- ion mean energy: 8 GeV
- beam radius R_{en} : 35 mm
- chamber radius: 2 – 8 m
- beam emittance: 3 – 10 mm-mrad

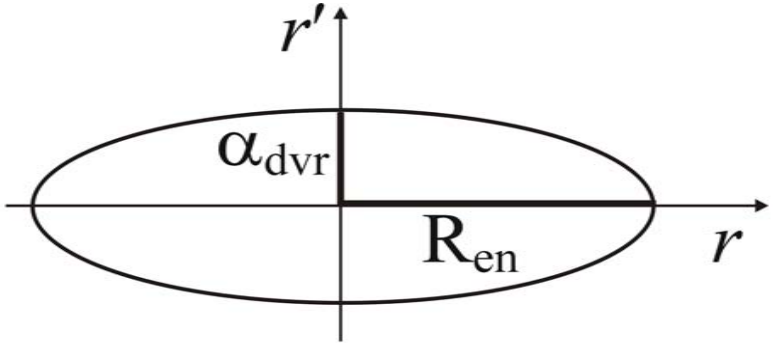

(a)

$$\varepsilon_r = \iint dr\, dr' = \pi\alpha_{dvr}R_{en} = \pi\frac{\pi\cdot 1000}{180}\alpha_{dvr}[\text{deg}]\cdot R_{en}[\text{mm}] = \frac{\pi^2}{0.18}\alpha_{dvr}R_{en}[\text{mm-mrad}]$$

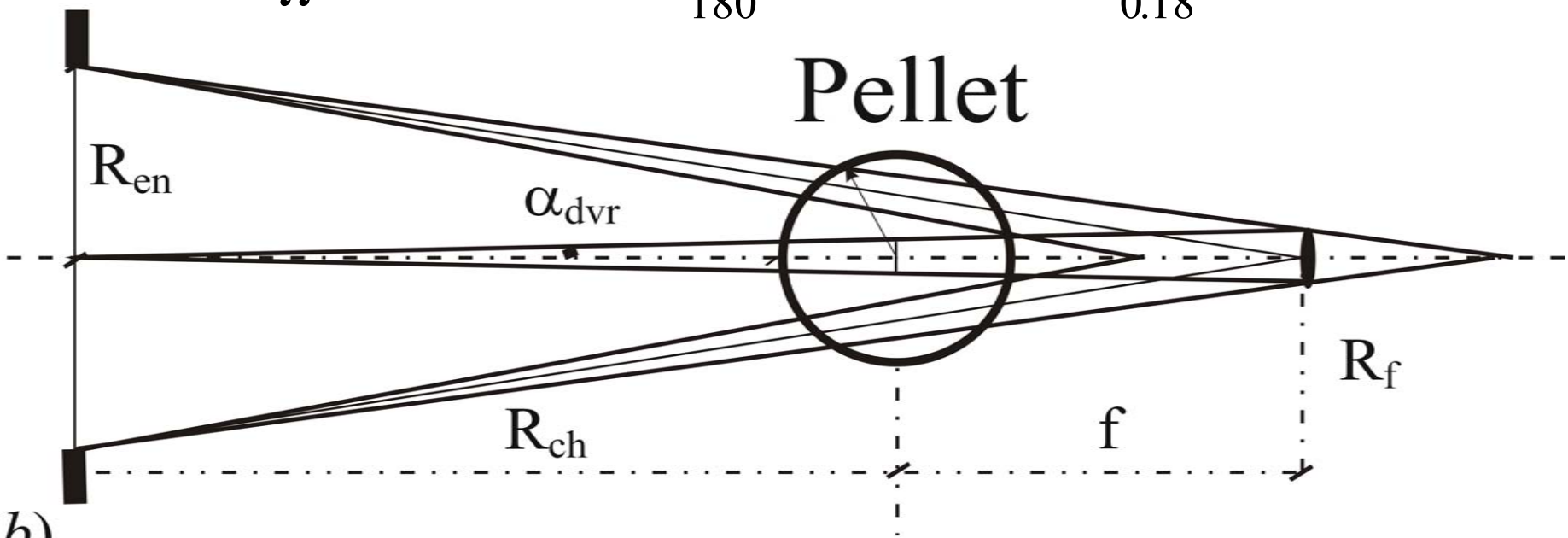

(b)

additional

OK2 Algorithm:

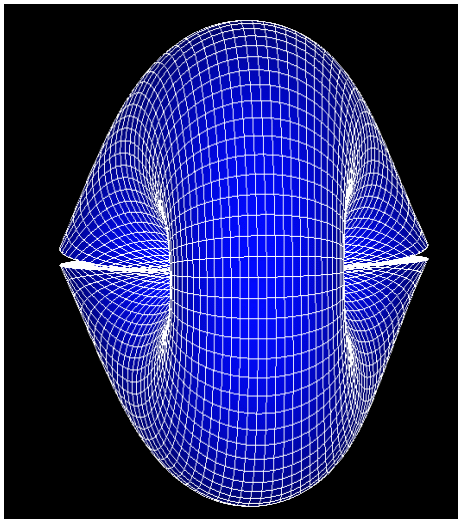

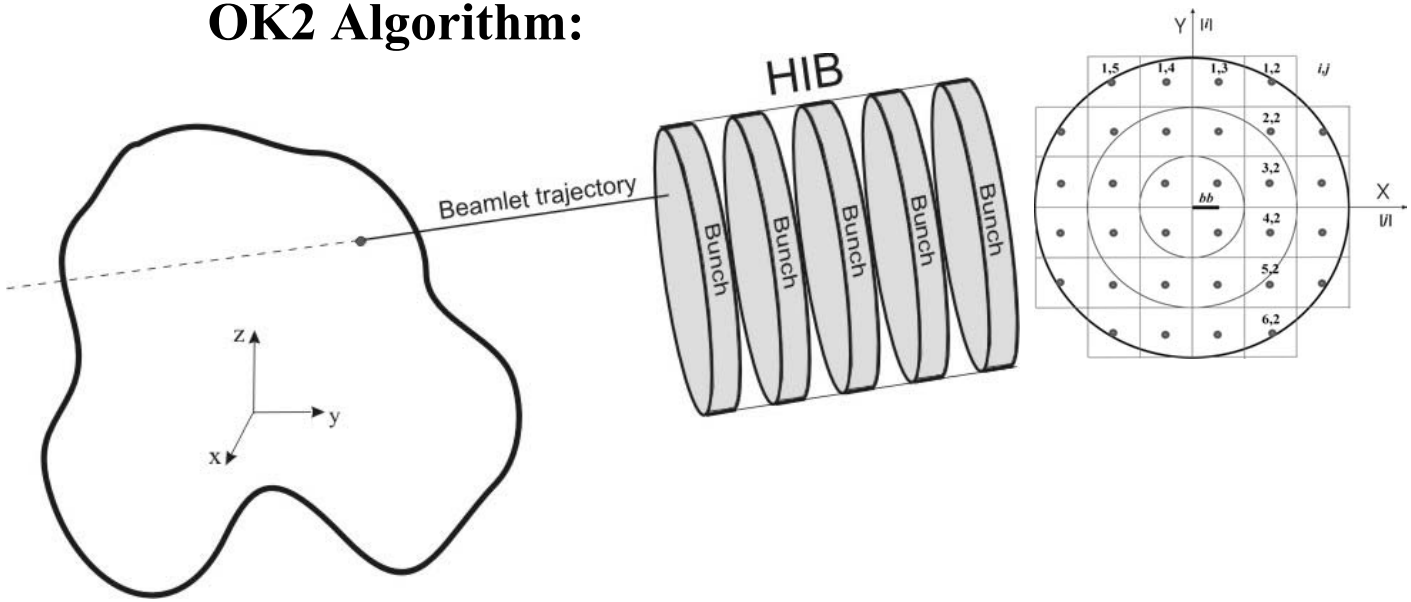

1) Initialize the beam and target parameters.
2) Take the first bunch.
3) Set the target temperature.
4) Take the first beam from the fixed irradiation scheme.
5) Divide the beam into multiple beamlets (32, 80, 112, 316,…) and take the first one.
6) Find the beamlet – target intersection and fix the beamlet direction.
7) Find all mesh centers inside the iterative cylindrical beamlet area and fill their corresponding meshes with the calculated energy density.
8) Make the next penetration step (till the completely beamlet energy deposition) and go to step 7.
9) Take the next beamlet (till the last one) and go to step 6.
10) Take the next beam (till the last one) and go to step 5.
11) Take the next bunch (till the last one) and go to step 3.
12) Save the results.
13) End.

additional

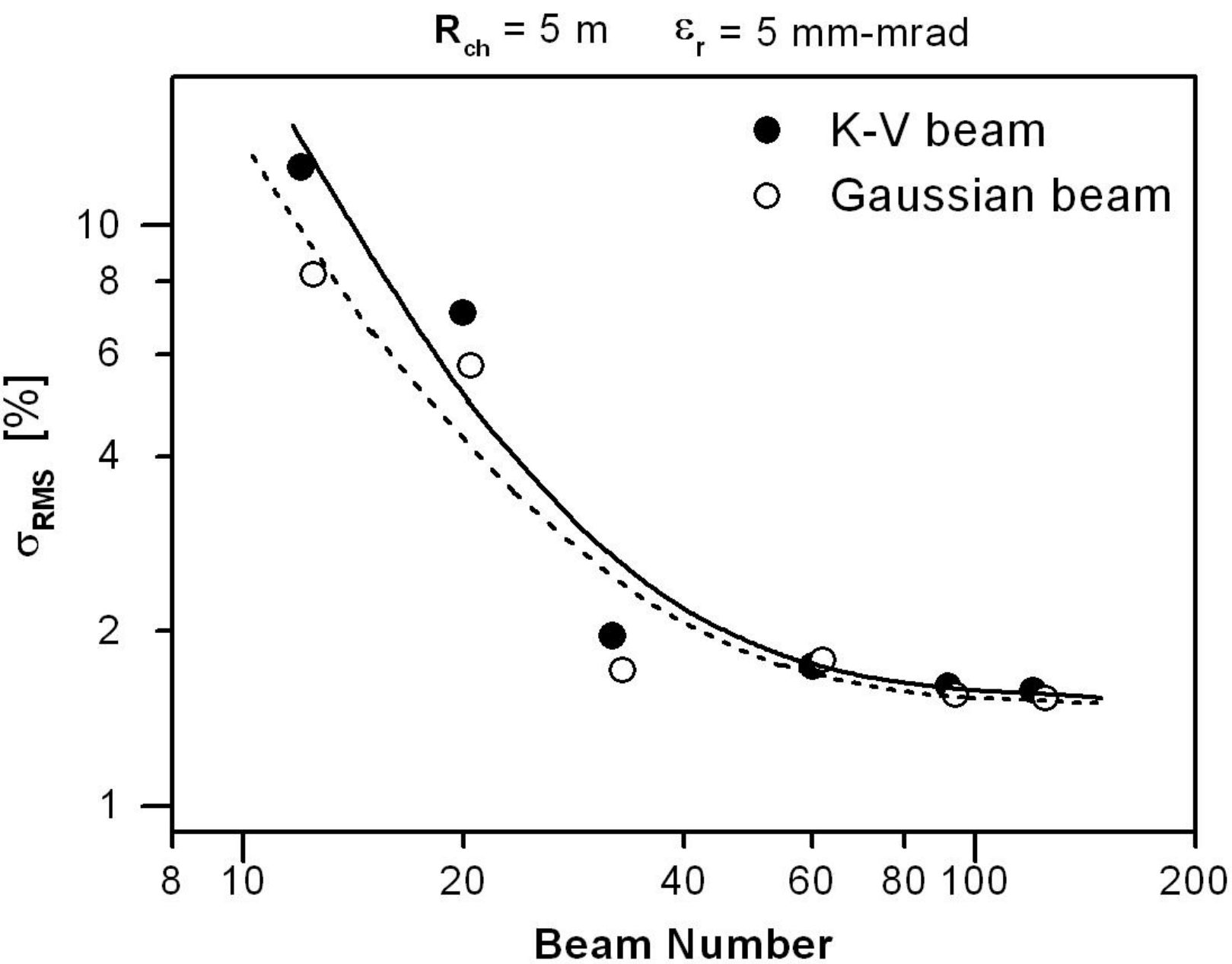
R_{ch} = 5 m
ε_r = 5 mm-mrad
K-V beam
Gaussian beam
σ_{RMS} [%]
10
8
6
4
2
1
8
10
20
40
60
80
100
200
Beam Number

additional

Beam number influence on the energy deposition uniformity

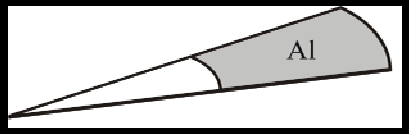

R_{ch} = 2 m ε_r = 10 mm-mrad

Al pellet

σ_{RMS}

σ_{PTV}

σ_{RMS} , σ_{PTV} [%]

10

1

10

100

Beam Number

additional

Reactor chamber radius dependence for fixed beam emittance

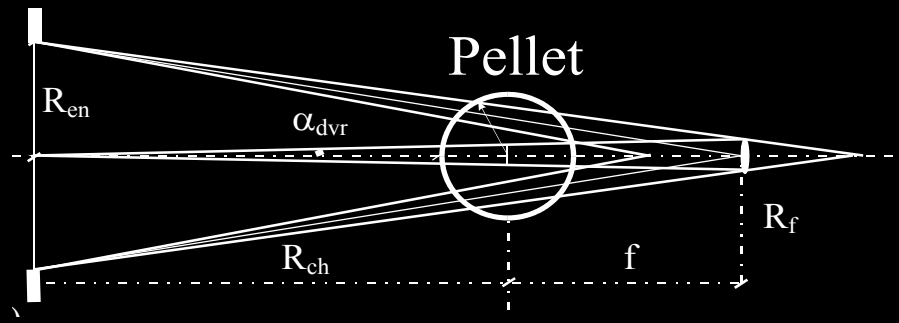

ε_r = 5 mm-mrad

f [m], R_f [mm]

1.0
0.5
0.0
f
Rf

σ_{RMS} [%]

5
4
3
2
1
32
60
120

1 2 3 4 5 6 7 8 9

Chamber radius [m]

additional

Reactor chamber radius dependence for fixed focal spot radius

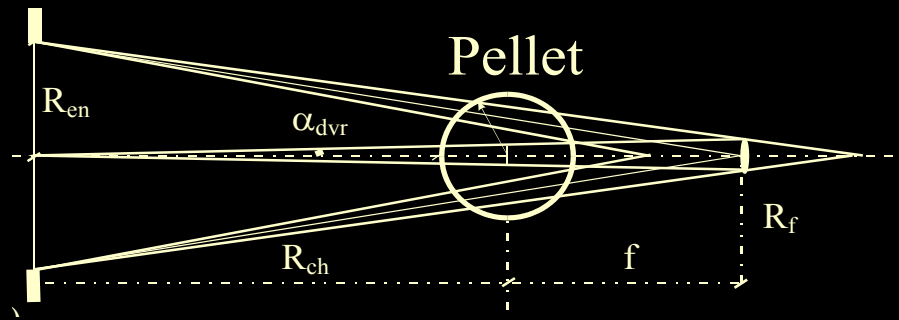

R_f = 0.66 mm

f [m]

ε_r [mm-mrad]

σ_{RMS}[%]

Chamber radius [m]

f
ε_r
32
60
120

additional

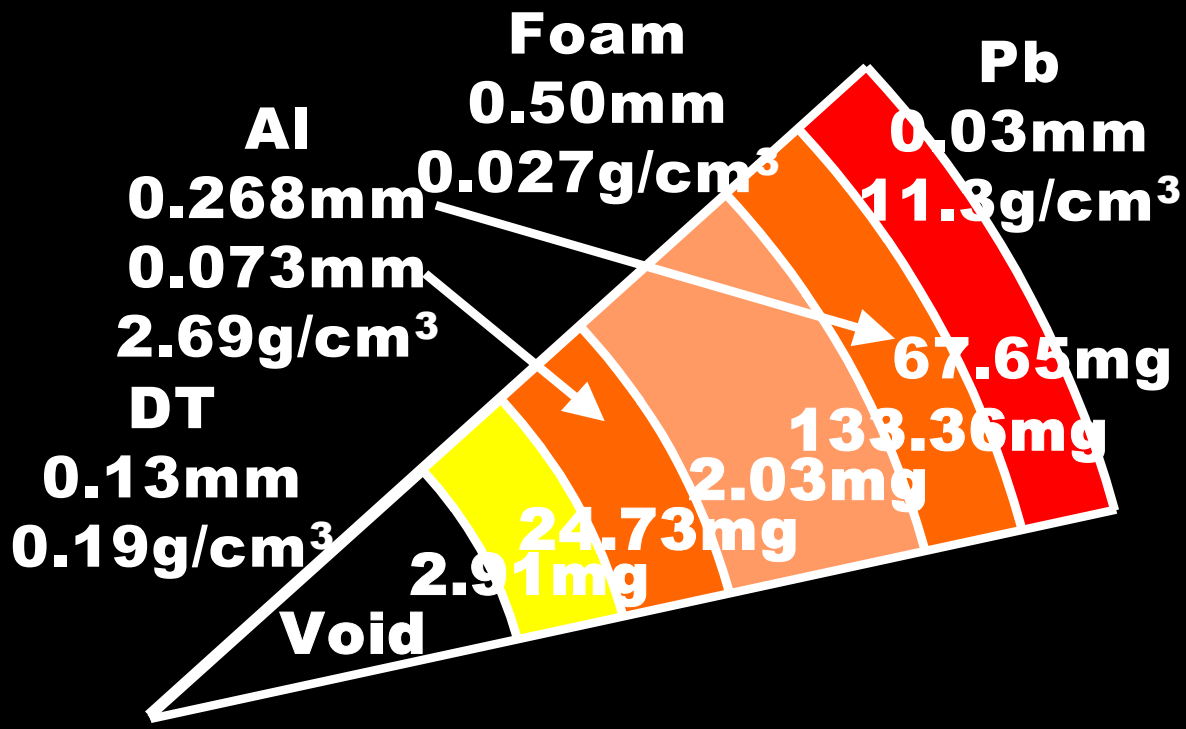
Foam
0.50mm
0.027g/cm³
Pb
0.03mm
11.3g/cm³
Al
0.268mm
0.073mm
2.69g/cm³
DT
0.13mm
0.19g/cm³
67.65mg
133.36mg
2.03mg
24.73mg
2.91mg
Void

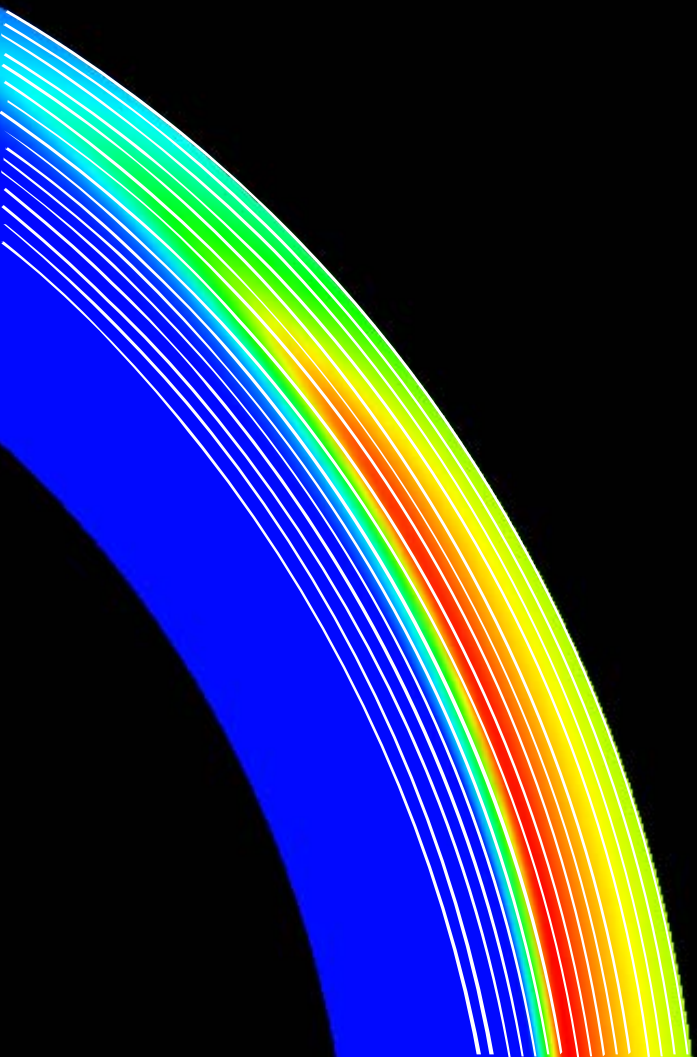

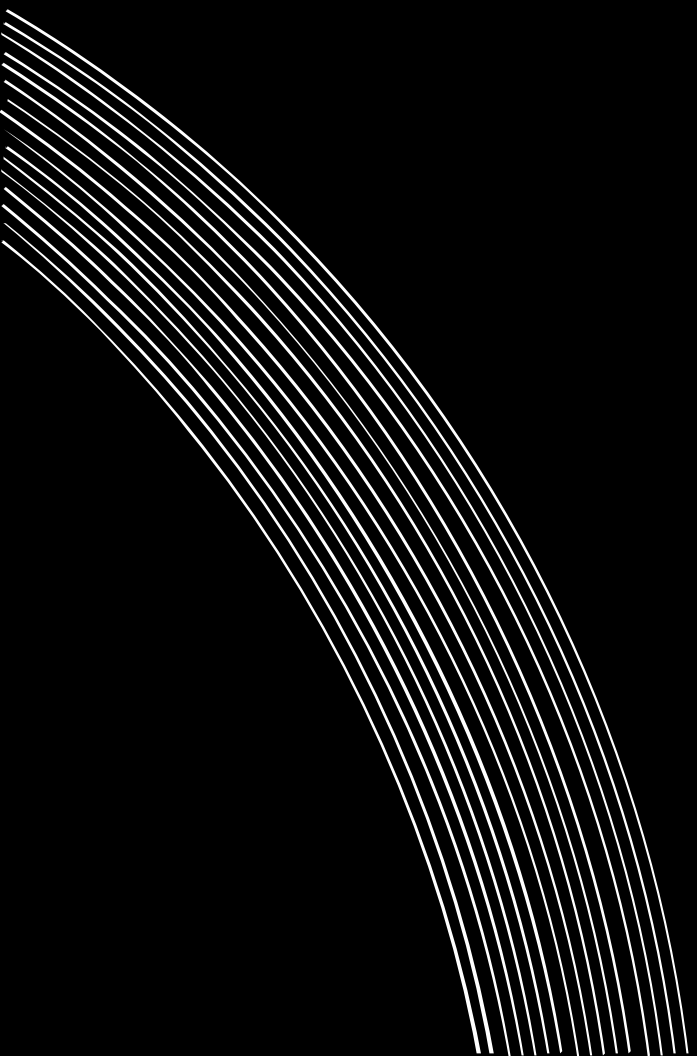

ICF modelling of interaction of large heavy ion beams with a target

A. I. Ogoyski [1] and S. Kawata [2]

[1] *Technical University of Varna, 9010 Varna, Bulgaria*
[2] *Utsunomiya University, Utsunomiya 321-8585, Japan*

Abstract

In heavy ion beam (HIB) inertial confinement fusion (ICF), implosion asymmetry should be less than a few percent in order to compress a fuel sufficiently and release fusion energy effectively. It is known that the HIB irradiation non-uniformity and implosion symmetry are sensitive to a little pellet displacement from the reactor chamber center. We present a new HIB irradiation scheme that is robust against the displacement of a direct-driven fuel pellet in heavy ion fusion (HIF) reactor chamber. In conventional HIB irradiation schemes, a pellet displacement of 60–70 μm was tolerable. The new OS-32 HIB irradiation scheme is examined by three-dimensional computer simulations. In that scheme the tolerable pellet displacement is about 300 μm.

PACS: 52.58.Hm; 52.40.Mj; 52.57.Fg; 29.27.Eg
Keywords: Heavy ion fusion; Beam illumination; Stopping power

Introduction

Due to a favorable energy deposition behavior of heavy ions in matter, high accelerator efficiency and recent research explorations [1–9], it is expected that HIBs would be one of energy driver candidates to operate a future ICF power plant. Preferable features in HIF include direct coupling of the HIB energy to a fuel pellet and relatively deep-area heating of an energy deposition layer. For successful fuel ignition and sufficient fusion energy release, a stringent requirement is imposed on the HIB irradiation non-uniformity, which should be less than a few percent.

In our study, the non-uniformity of HIB irradiation onto a direct-driven spherical fuel pellet in HIF is investigated numerically. We evaluate and analyze the HIB energy deposition non-uniformity using 12, 20, 32, 60, 92 and 120 beam irradiation systems, including effects of HIB emittance, magnitude of the reactor chamber radius, HIB density distribution and little pellet displacement from the chamber center.

Previous researches [9–12] show that a little pellet displacement from the reactor chamber center should be less than about 60–70 μm. If this requirement is relaxed, the target placement precision, the driver HIB alignment accuracy, and the target tracking accuracy may be also relaxed. The new proposed OS-32 irradiation scheme is robust against the fuel pellet displacement of about 300 μm.

Stopping power model

The main purpose is creation of temperature dependent stopping power model.

The one-ion stopping power is considered to be a sum of the energy deposited in target nuclei, target bound and free electrons and target ions [6].

$$E_{StPower} = E_{nuc} + E_{bound} + E_{free} + E_{ion} \quad (1)$$

The nuclear stopping power process is effective in the end of the stopping range and describes the elastic Coulomb collisions between the projectile ions and target nuclei [13,14]:

$$\mathrm{E_{nuc}} = 10^{-7} C_{n1} \sqrt{E} \exp\left(-45.2 (C_{n2} E)^{0.277}\right), \tag{2}$$

$$C_{n1} = 4.14 \times 10^{6} \rho \left(\frac{\mathrm{A_b}}{\mathrm{A_b + A_t}}\right)^{3/2} \left(\frac{\mathrm{Z_b Z_t}}{\mathrm{A_b}}\right)^{1/2} \left(\mathrm{Z_b}^{2/3} + \mathrm{Z_t}^{2/3}\right)^{-3/2}, \tag{3}$$

$$C_{n2} = 10^{-6} \rho \left(\frac{\mathrm{A_b A_t}}{\mathrm{A_b + A_t}}\right)^{3/2} (\mathrm{Z_b Z_t})^{-1} \left(\mathrm{Z_b}^{2/3} + \mathrm{Z_t}^{2/3}\right)^{-1/2}, \tag{4}$$

where A_b and A_t are the projectile and target atomic weights, Z_b and Z_t – the projectile and target atomic numbers, E – the projectile ion energy and ρ – the target density.

The Linhard and Bethe–Bloch equations describe the bound electron stopping power process. The model uses the Thomas–Fermi description of the electron clouds and includes the Coulomb collisions as well as excitation and ionization processes [13–16]:

$\mathrm{E_{bound}} = \mathrm{E_{LSS}}\ \mathbf{U}\ \mathrm{E_{Bethe}}$, with LSS validity criterion: $\mathrm{Z_b^{1/3}} \geq 137 \frac{\mathrm{V_{beam}}}{c}$, (5)

$$\mathrm{E_{LSS}} = \frac{2e^2 a_B n_{eb}}{e_0 V_B} \frac{\mathrm{Z_b^{7/6}}}{\left(\mathrm{Z_b^{2/3} + Z_t^{2/3}}\right)^{3/2}} \mathrm{V_{beam}}$$, (aB and VB are the Bohr radius and velocity), (6)

$$\mathrm{E_{Bethe}} = \frac{e^4 n_{eb}}{4\pi e_0^2 m_e} \frac{Zeff_b^2}{\mathrm{V_{beam}^2}} \left[\ln \frac{2 m_e \mathrm{V_{beam}^2}}{\langle U_i \rangle} - \ln(1-b) - b - d\right], \quad b = \frac{\mathrm{V_{beam}^2}}{c^2}. \tag{7}$$

The effective projectile charge is

$$Zeff_b = \mathrm{Z_b}\left(1 - 1.034 \exp\left(-137.04 \frac{1}{\mathrm{Z_b^{0.69}}} \frac{\mathrm{V_{beam}}}{c}\right)\right) \tag{8}$$

by the Brown and Moak expression [6–17]. The shell corrections coefficients d and the average ionization potential $\langle U_i \rangle$ of the target are taken from Andersen and Ziegler [13]. The temperature dependence of target ionization $Z_t(T)$ is obtained solving the equation of state (EOS) based on the Thomas-Fermi model [18]. The ionization of Al target as a function of temperature and particle number density is evaluated (Fig.1), and interpolated for a fixed solid-state density (Fig.2).

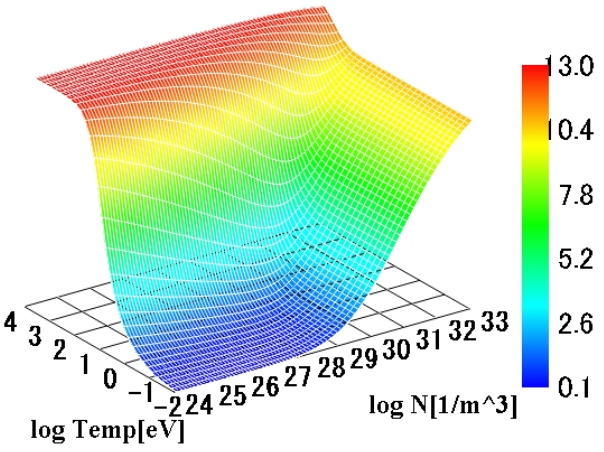

Fig.1

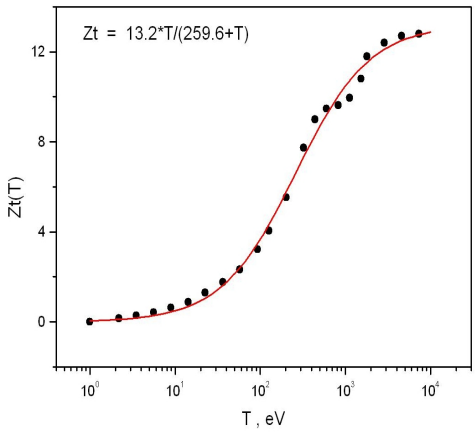

Fig.2

The free electron stopping power becomes effective with target temperature growth [4,5].

$$\mathrm{E}_{\mathrm{free}} = \frac{e^4 n_{\mathrm{ef}}}{4pe_0^2 m_{\mathrm{e}}} \frac{Zeff_{\mathrm{b}}^2}{\mathrm{Vr}_{\mathrm{e}}^2} \left(G_{\mathrm{e}} L_{\mathrm{e}} + H_{\mathrm{e}}\right), \tag{9}$$

$$G_{\mathrm{e}} = \mathrm{erf}\left(\frac{\mathrm{X}_{\mathrm{e}}}{\sqrt{2}}\right) - \sqrt{\frac{2}{p}} \mathrm{X}_{\mathrm{e}} \exp\left(-\frac{\mathrm{X}_{\mathrm{e}}^2}{2}\right) \quad \text{is the Chandrasekhar function,} \quad \mathrm{X}_{\mathrm{e}} = \frac{\mathrm{Vr}_{\mathrm{e}}}{\mathrm{V}_{\mathrm{e}}}, \tag{10}$$

$$L_{\mathrm{e}} = \ln\left(\frac{l_{\mathrm{D}}}{b_{\min}}\right), \quad H_{\mathrm{e}} = -\frac{\mathrm{X}_{\mathrm{e}}^3}{3\sqrt{2p}\,\ln \mathrm{X}_{\mathrm{e}}} \exp\left(-\frac{\mathrm{X}_{\mathrm{e}}^2}{2}\right) + \frac{\mathrm{X}_{\mathrm{e}}^4}{\mathrm{X}_{\mathrm{e}}^4 + 12}. \tag{11}$$

Here n_{ef} is the free electron number density, Vr_{e} is the relativistic projectile velocity, V_{e} is the electron thermal velocity, $b_{\min}$ is the distance of closest approach and l_{D} is the Debye length.

The free ion stopping power is described analogically by Eqs. 12, 13 and 14.

$$\mathrm{E}_{\mathrm{ion}} = \frac{e^4 n_{\mathrm{a}}}{4pe_0^2 M_{\mathrm{t}}} \frac{Zeff_{\mathrm{b}}^2 \mathrm{Z}_{\mathrm{t}}^2}{\mathrm{V}_{\mathrm{beam}}^2} \left(G_{\mathrm{i}} L_{\mathrm{i}} + H_{\mathrm{i}}\right), \tag{12}$$

$$G_{\mathrm{i}} = \mathrm{erf}\left(\frac{\mathrm{X}_{\mathrm{i}}}{\sqrt{2}}\right) - \sqrt{\frac{2}{p}} \mathrm{X}_{\mathrm{i}} \exp\left(-\frac{\mathrm{X}_{\mathrm{i}}^2}{2}\right), \quad \mathrm{X}_{\mathrm{i}} = \frac{\mathrm{V}_{\mathrm{beam}}}{\mathrm{V}_{\mathrm{i}}}, \tag{13}$$

$$L_{\mathrm{i}} = \ln\left(\frac{l_{\mathrm{D}}}{b_{\min}}\right), \quad H_{\mathrm{i}} = -\frac{\mathrm{X}_{\mathrm{i}}^3}{3\sqrt{2p}\,\ln \mathrm{X}_{\mathrm{e}}} \exp\left(-\frac{\mathrm{X}_{\mathrm{i}}^2}{2}\right) + \frac{\mathrm{X}_{\mathrm{i}}^4}{\mathrm{X}_{\mathrm{i}}^4 + 12}, \tag{14}$$

M_{t} is the target atomic mass, n_{a} is the target atom number density and V_{i} is the ion thermal velocity.

The stopping power curves for one Pb projectile ion in an Al target in a temperature range of 1eV – 1KeV are plotted in Fig.3, and compared with Mehlhorn's [6] and Ziegler's [13] data for energy deposition in cold target.

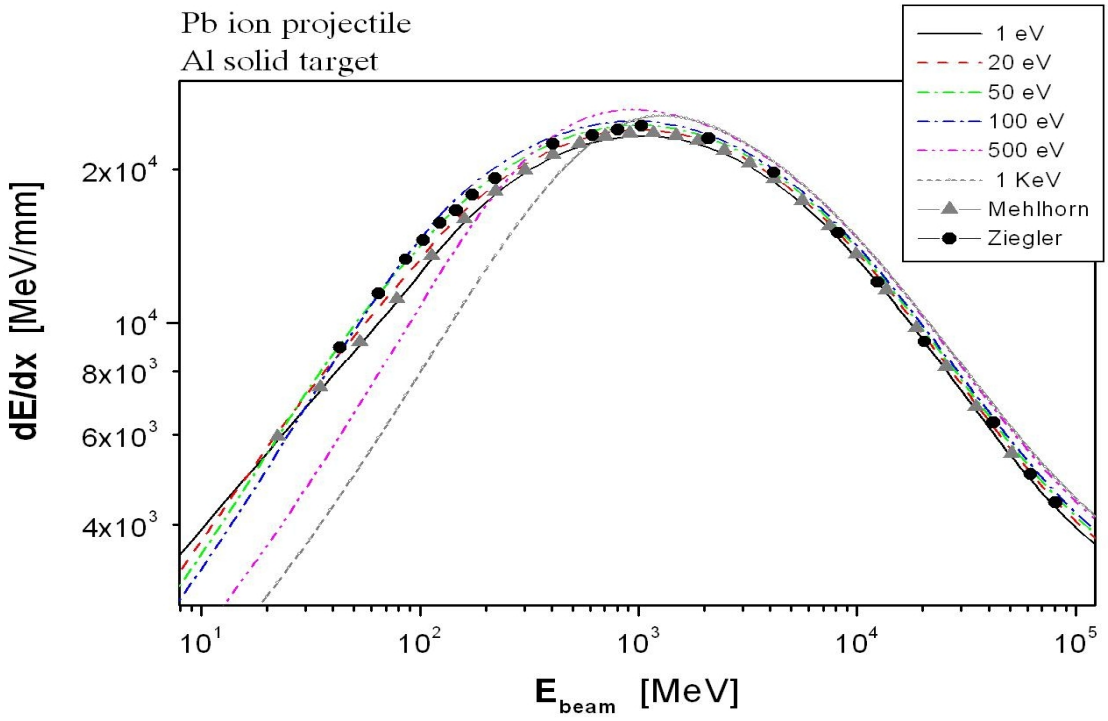

Fig.3

Target temperature model

The main purpose is to simulate the temperature growth during the time of irradiation. The first impinging ions heat the pellet surface, the temperature rises and the following projectile ions meet different stopping power conditions.

The energy balance equation (15) is solved and the pellet temperature T_m at the end of the deposition period is found.

$$
\begin{aligned}
& N_b E_b = E_{dst} + E_i + E_{rad} + n_{Al} V_{dp} \frac{3}{2}(T_m - T_0) \\
& E_{dst} = n_{Al} V_{dp} E_{cpl} \\
& E_i = n_{Al} V_{dp} \langle I \rangle \frac{1}{T_m - T_0} \int_{T_0}^{T_m} Z(T) dT \\
& E_{rad} = sS \int_0^{t_{dp}} T^4(t) dt \\
& Z(T) = \frac{13.2\ T}{259.6 + T}
\end{aligned}
\qquad (15)
$$

N_b is the number of beams, E_b is the energy of one beam, E_{dst} is the energy loss for destruction of the initial pellet crystal state, E_{cpl} is the energy coupling of one Al atom, n_{Al} is the pellet atom density, V_{dp} is the volume of deposition, E_i is the ionization loss, $\langle I \rangle$ is the mean ionization potential of Al, E_{rad} is the radiation loss across the pellet surface S and s is the Stephan-Boltzmann constant. The pellet ionization $Z(T)$ is evaluated by solving the EOS using Thomas-Fermi model for Al and interpolating the results for a fixed solid-state density (Fig.2). The results for the target temperature T_m at the end of deposition versus the number of impinging beams are plotted on Fig.4.

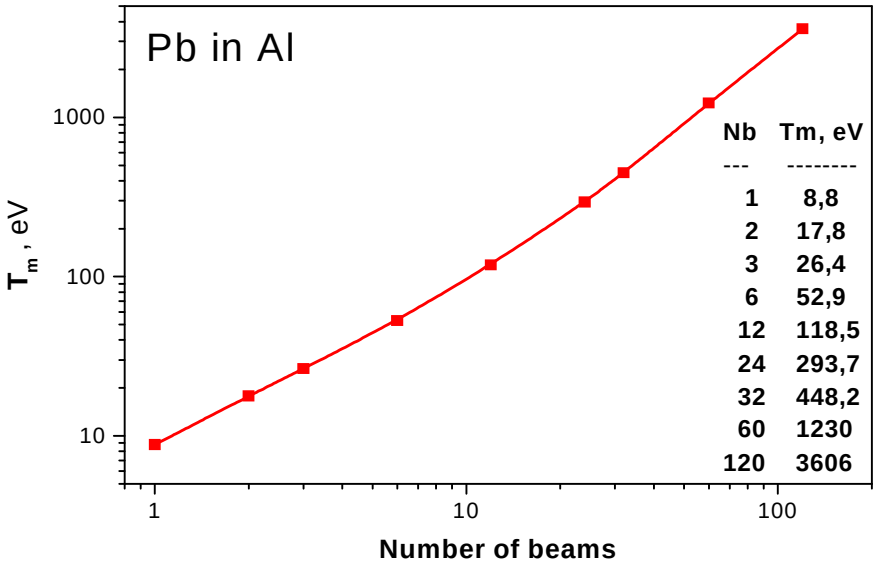

Fig.4

In the recent simulation model (32-beam irradiation), we assume a linear temperature growth during the time of deposition from 0.025 eV to 448 eV.

Simulation results

The Al pellet is irradiated by 12, 20, 32, 60, 92 and 120-beam central–symmetric systems. We employ Pb^+ ion beams with the mean particle energy of 8 GeV. The beam particle density distribution in one beam is the Kapchinski–Vladimirski (KV) distribution and the Gaussian. The longitudinal temperature of projectile ions is 100 MeV with the Maxwell distribution. The beam radius R_{en} at the entrance of the reactor chamber is 35 mm. The chamber radius R_{ch} varies from 2 to 8 m. The beam-focusing scheme (Fig.5) determines the focal spot distance f and radius R_f. The beam emittance e_r varies from 3 to 10 mm-mrad.

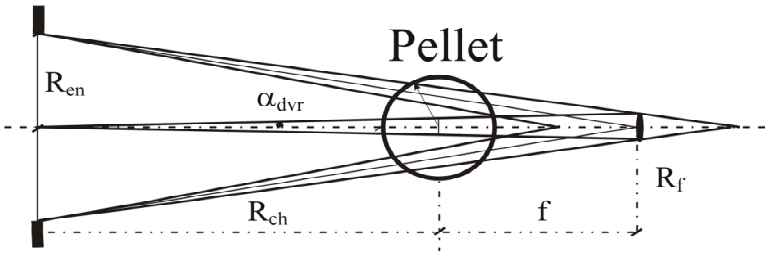

Fig.5

Example energy deposition profiles of one HIB in the KV and Gaussian distributions in an Al monolayer pellet are shown in Fig.6(*a*) and (*b*).

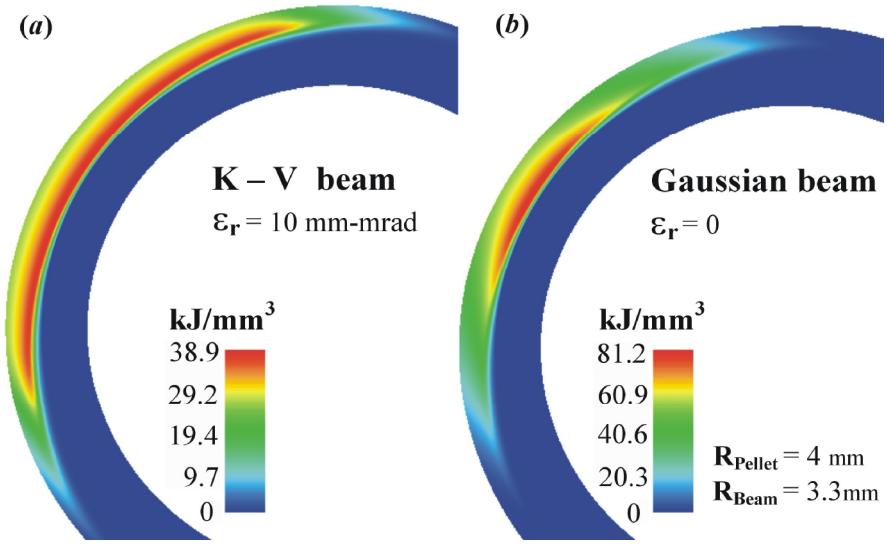

Fig.6

The energy deposition layer has external radius R_0 = 4mm and thickness of 1mm. It is divided into a mesh structure in the r, q and f directions with the following mesh numbers: $n_r = 100$, $n_q = 90$, $n_f = 90$. Each spherical shell layer has a thickness dr of 0.01 mm. The Bragg peak area plays the most substantial role for a uniform fuel pellet implosion in HIF, so that the uniformity of the Bragg peak radial position is important as well as the uniformity of the HIB energy deposition profile along the surface. Therefore, we define the total relative root-mean-square (RMS) deviation as follows:

$$s_{\mathrm{RMS}} = \sum_i^{n_r} w_i s_{\mathrm{RMS}\,i}\ , \qquad s_{\mathrm{RMS}\,i} = \frac{1}{\langle E \rangle_i}\sqrt{\frac{\sum_j^{n_q}\sum_k^{n_f}\left(\langle E \rangle_i - E_{ijk}\right)^2}{n_q n_f}}\ , \qquad w_i = \frac{E_i}{E}\ , \tag{16}$$

where $s_{RMS\,i}$ is the relative RMS deviation on the *i*-the deposition shell, E_i is the energy deposited on that shell and E is the total energy deposition. Fig.7 shows a dependence of s_{RMS} on the total HIB number employed in the Al monolayer target, irradiated by 12, 20, 32, 60, 92 and 120 HIBs with central-symmetric polyhedron structures for the KV and Gaussian HIBs.

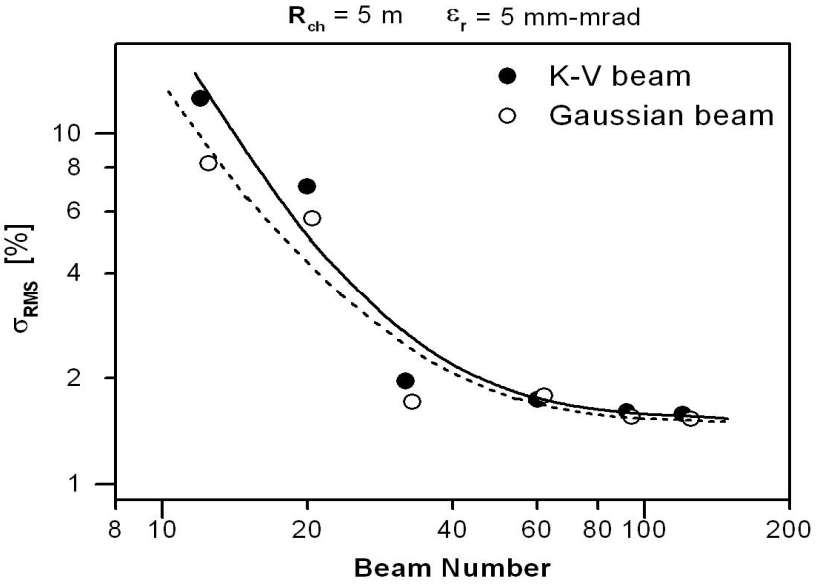

Fig.7

The simulation results demonstrated that a sufficiently low non-uniform energy deposition (less than 2%) can be realized with a finite number of beams and determined a 32-beam irradiation system as most interesting for practical application.

Pellet displacement sensitivity

The simulation results suggest that the HIB irradiation non-uniformity is sensitive to a little pellet displacement from the chamber center (Fig.8).

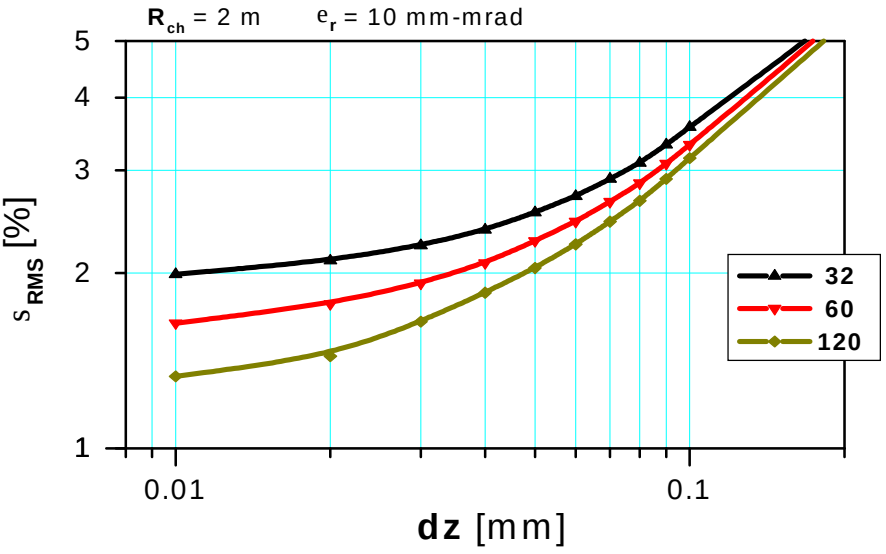

Fig.8

In 32-beam irradiation, a pellet displacement of 60-70 μm causes non-uniformity growth of 1%. Farther pellet displacement is not acceptable and will result in low-efficient implosion and unsuccessful fusion. Therefore, it is very important the requirement of target placement precision to be relaxed. Then the driver HIB alignment accuracy and the target tracking accuracy may be also relaxed. The new proposed OS-32 irradiation scheme is robust against fuel pellet displacements of about 300 μm.

OS-32 axial symmetric scheme of large HIBs

The idea to decrease the pellet displacement sensibility by using OS-32 irradiation scheme consists in two essential points:

1) Using of large ion beams which radius on a tangential to the pellet surface plane should be greater than the pellet radius.

2) Modifying OMEGA-32 irradiation scheme from spherical symmetric, to axial symmetric in order to obtain an ellipsoidal area in the reactor chamber, where the energy deposition non-uniformity to remain nearly constant if the pellet is inside (Fig.9).

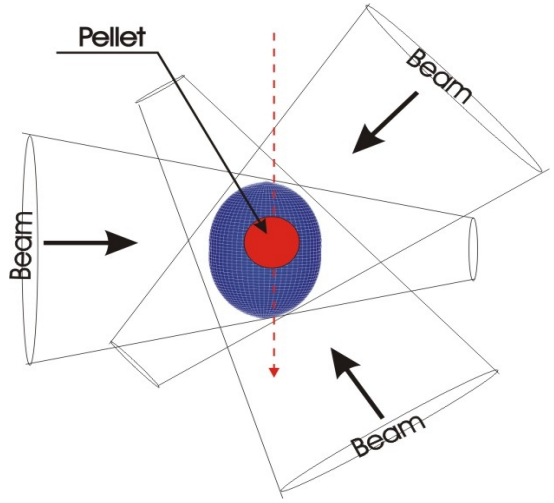

Fig.9

OMEGA-32 irradiation scheme has a central-symmetric polyhedron structure [19]. The centers of HIBs on a target surface are plotted in Fig.10.

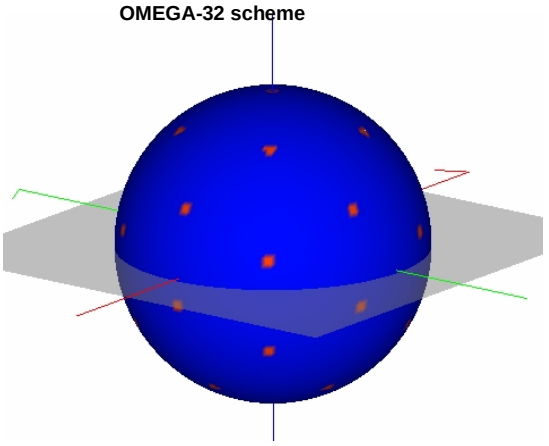

Fig.10

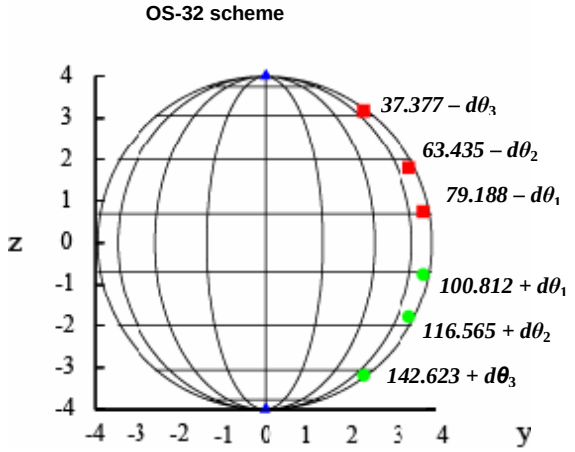

Fig.11

OS-32 axial symmetric scheme is obtained from OMEGA-32 by shifting HIB impinging directions to angles dq_1, dq_2, dq_3 (in spherical coordinates r, q, f), as shown in Fig.11. HIB radii have been enlarged to 5,6 mm near to the pellet surface. Pellet radius is 4mm. The energy deposition non-uniformities s_{RMS} versus the pellet displacement *dz* for OMEGA-32 and OS-32 schemes are compared in Fig.12. Using OMEGA-32 irradiation scheme, a pellet

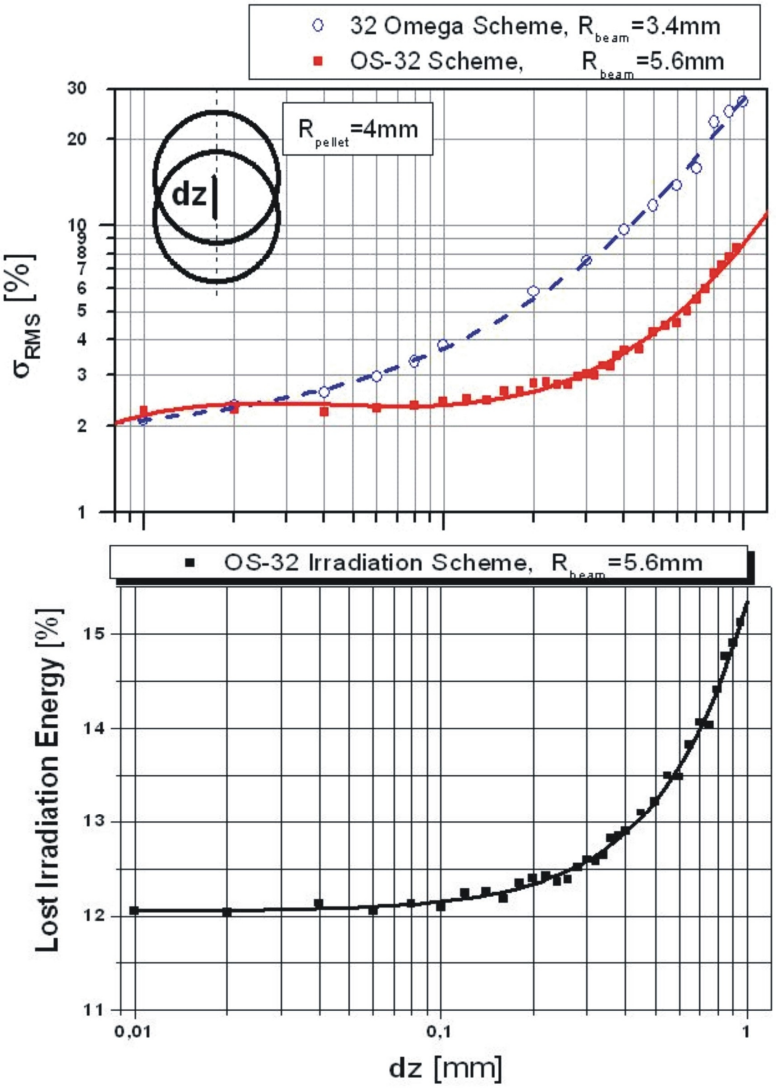

Fig.12

displacement of about 60-70 μm causes non-uniformity growth of 1%. In OS-32 irradiation scheme, pellet displacements of 300 μm are admissible. However, the lost irradiation energy due to the large HIB radii is about 12 – 13%.

These simulation results were confirmed by Japanese colleagues in Kawata Lab at Utsunomiya University, Japan [20]. OS-32 irradiation scheme was improved by reducing HIB radii from 5,6 mm to 4,6 mm and declination angle Δq from 4 to 2 degrees, in order to minimize the HIB energy lost. Systematic simulations using 12 and 20-beam schemes were performed too (Fig.13). A pellet structure with an external thin lead tamper layer slightly increases the energy deposition non-uniformity, but does not affect the displacement sensibility.

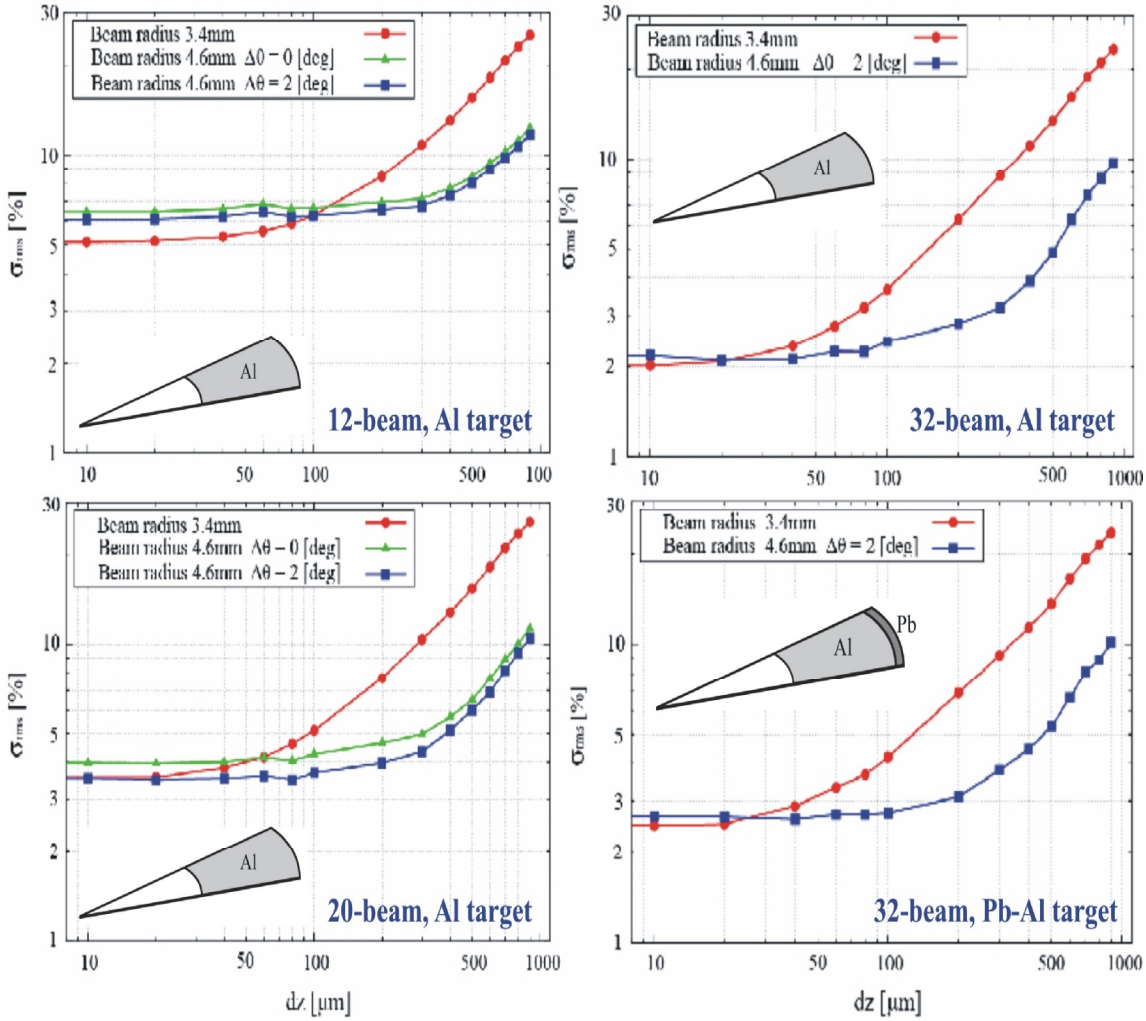

Fig.13

Conclusions

1. Three-dimensional computer codes OK1, OK1c and OK2 were developed for simulation of multi HIB irradiation on a spherical, cylindrical and arbitrary shaped fuel pellet.

2. A 3D criterion for non-uniformity estimation was established.

3. We investigated the energy deposition non-uniformity dependence on:
   - reactor chamber radius,
   - beam focusing,
   - beam emittance,
   - beam number irradiation system,
   - little pellet displacement from the reactor chamber center.

4. A 32-beam irradiation scheme has been confirmed the most interesting for the future HIF practice.

5. A new OS-32 HIB axial symmetric irradiation scheme is proposed, robust against pellet displacement from the reactor chamber center.

References

[1] J.J. Barnard et al., LLNL Research Report, UCRL-LR-108095 (1991).
[2] C. Deutsch, et al., J. Plasma Fusion Res. 77, 33 (2001).
[3] M. Roth, et al., Europhys. Lett. 50, 28 (2000).
[4] T. Peter, J. Meyer-ter-Vehn, Phys. Rev. A 43, 1998 (1991).
[5] T. Peter, J. Meyer-ter-Vehn, Phys. Rev. A 43, 2015 (1991).
[6] T. Mehlhorn, Sandia Report, SAND80-0038, (1980).
[7] D.H.H. Hoffmann, et al., Phys. Rev. A 42, 2313 (1990).
[8] M. Reiser, Wiley, New York, (1994).
[9] A.I. Ogoyski, T. Someya, T. Sasaki, S. Kawata, Phys. Let. A, Vol. 315, 372-377 (2003).
[10] T. Someya, A.I. Ogoyski, S. Kawata, T. Sasaki, Phys. Rev. ST Accel. Beam 7 (2004).
[11] T. Someya, S. Kawata, T. Kikuchi, A.I. Ogoyski, Nucl. Instr. And Meth. A 544 (2005).
[12] D.T. Goodin, et al., Fusion Eng. Des. 60 (2002).
[13] H.H. Andersen and J.F. Ziegler, 3 (Pergamon Press, 1977).
[14] P. Wang, et al., Phys. Plasmas, 5, 2977 (1998).
[15] F.C. Young et al., Phys. Rev. Lett. 49, 549 (1982).
[16] K.A. Long and N.A. Tahir, Phys. Lett. A 91, 451 (1982).
[17] J.A. Swegle, Sandia Report, SAND82-0072, (1982).
[18] A.R.Bell, Rutherford Laboratory Report, RL-80-091, (1981).
[19] S. Skupsky, K. Lee, J. Appl. Phys. 54, 3662 (1983).
[20] S. Kawata, et al, Nuclear Instr. and Methods in Phys. Res. A **577**, 327-331 (2007).